JOURNAL OF GEOPHYSICAL RESEARCH, VOL. 112, B01202, doi:10.1029/2006JB004342, 2007

Crystallization pressures of mid-ocean ridge basalts derived from major element variations of glasses from equilibrium and fractional crystallization experiments

Samuel Villiger,[1] Othmar Müntener,[2,3] and Peter Ulmer[1]

Received 13 February 2006; revised 5 September 2006; accepted 13 September 2006; published 17 January 2007.

[1] A new method for calculating fractionation pressures of mid-ocean ridge basalts (MORB) that are saturated in clinopyroxene and plagioclase is presented. This mineral assemblage is the major control on the CaO versus Mg # (molar Mg/(Mg + Fe_{tot}), all Fe as Fe^{2+}) chemical variations of basaltic liquids. By combining new equilibrium and fractional crystallization experiments on primitive mid-ocean ridge basalts at high pressure with previously published experiments on natural basaltic systems, we derive an expression for fractionation pressures that depends only on the CaO content and the Mg # of the liquid. P (kbar) = [CaO (wt %) − 3.98(±0.17) − 14.96(±0.34) × Mg # (molar)]/[−0.260(±0.008)], $r^2 = 0.92$. We compare our formulation of a liquid barometer with those of Grove et al. (1992), Yang et al. (1996), and Herzberg (2004). The equation can be used to predict crystallization pressures of dry tholeiitic liquids with Mg # < 0.6. Low H_2O contents in the liquid (<1 wt %) do not significantly affect the calculated pressures compared to anhydrous liquids. Pressure calculations have been performed on MORB glasses for three mid-ocean ridge systems with different spreading rates (East Pacific Rise, Mid-Atlantic Ridge, Southwest Indian Ridge). Average pressure estimates correlate negatively with spreading rate when the MORB data are filtered for hot spot-affected compositions. Major element variations indicate that MORB crystallizing at elevated pressures also require lower degrees of mantle partial melting. Locations and compositions of MORB glasses crystallized at elevated pressures can be explained with models where conductive cooling is enhanced, either at segmented ridges with slow spreading rates or along ridge segment terminations at fast spreading ridges.

Citation: Villiger, S., O. Müntener, and P. Ulmer (2007), Crystallization pressures of mid-ocean ridge basalts derived from major element variations of glasses from equilibrium and fractional crystallization experiments, *J. Geophys. Res.*, *112*, B01202, doi:10.1029/2006JB004342.

1. Introduction

[2] Mid-ocean ridge basalts (MORB) are the most common eruptive products on the Earth's surface. It is generally accepted that they are generated by variable amounts of partial melting of mantle peridotite during adiabatic decompression. The extent of melting is mainly controlled by mantle potential temperature and peridotite source composition [e.g., *Klein and Langmuir*, 1987; *Langmuir et al.*, 1992; *Hirth and Kohlstedt*, 1996]. Most MORB compositions have Mg # lower than 0.7 and follow low-pressure cotectics, which is not consistent with a primary mantle origin [*Elthon and Scarfe*, 1984; *Grove et al.*, 1992]. Therefore primary mid-ocean ridge magmas must have experienced modification after extraction from a partially molten peridotite. One of the most important modification processes affecting mantle-derived basaltic liquids is fractionation at variable depths during their ascent from the source region to the surface. Mid-ocean ridge basalts preserve inherited chemical signatures of different mantle sources, melting processes and postmelting modifications [e.g., *Grove et al.*, 1992; *Sobolev and Shimizu*, 1993; *Spiegelman and Kelemen*, 2003]. To clarify one parameter of the compositional complexity of basalts, we focus on the fractionation process at variable depth below mid-ocean ridges.

[3] Previous experimental studies with basaltic bulk compositions [*Elthon*, 1979; *Elthon and Scarfe*, 1984; *Tormey et al.*, 1987; *Bartels et al.*, 1991; *Kinzler and Grove*, 1992; *Grove et al.*, 1992; *Yang et al.*, 1996] determined anhydrous phase relations and compositions of basalts at different pressures between 1 bar and 1.6 GPa. By mapping out the olivine (ol) − clinopyroxene (cpx) − plagioclase (plg) saturation surfaces of anhydrous basalts, two different quantitative models were developed to describe liquid compositions over a range of pressure, temperature and composition [*Grove et al.*, 1992; *Yang et al.*, 1996]. *Michael*

---

[1] Department of Earth Sciences, ETH Zürich, Zürich, Switzerland.
[2] Institute of Geological Sciences, University of Bern, Bern, Switzerland.
[3] Now at Institute of Mineralogy and Geochemistry, University of Lausanne, Lausanne, Switzerland.

0148-0227/07/2006JB004342$09.00

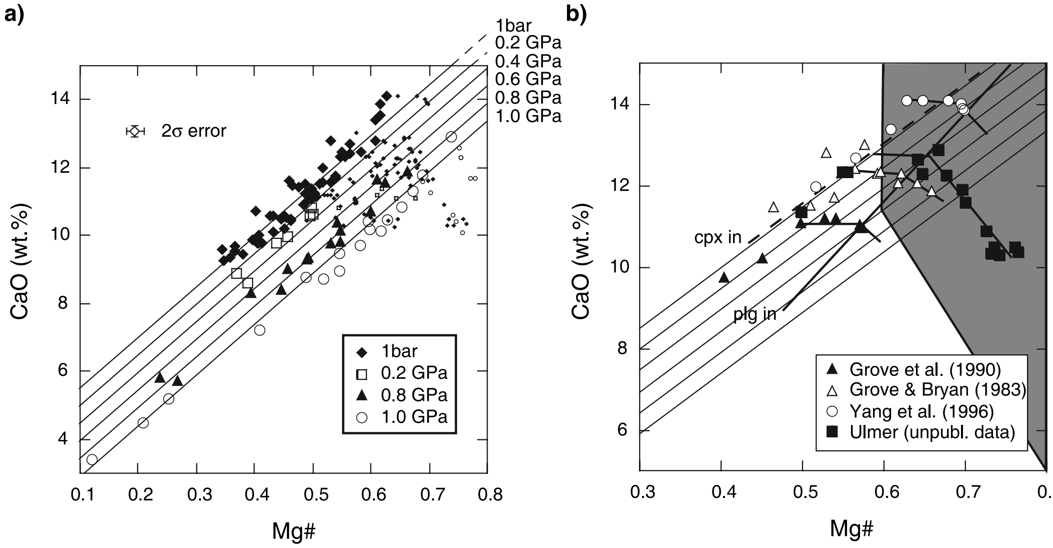

Figure 1. (a) Variation diagram CaO in wt % plotted against Mg # (= Mg/(Mg + Fe), all Fe as Fe^{2+}) of glass compositions (normalized to 100%) from selected anhydrous experiments saturated in cpx (±ol, plg, opx, spi). Experimental glasses in equilibrium with ol or ol + plg (±spi) are plotted as small symbols. Experimental data are from the following sequence: at 1 bar from *Grove and Bryan* [1983], *Tormey et al.* [1987], *Grove et al.* [1990], *Yang et al.* [1996], *Sano et al.* [2001], P. Ulmer (unpublished Data, 2004), at 0.2 GPa from *Tormey et al.* [1987] and *Grove et al.* [1992], at 0.8 GPa from *Baker and Eggler* [1987], *Grove et al.* [1990], and *Grove et al.* [1992], and at 1.0 GPa from *Fram and Longhi* [1992], *Grove et al.* [1992], and *Villiger et al.* [2004]. The error bars indicate the average of 2σ errors of 1.0 GPa glass analysis. (b) CaO plotted against Mg # of glass compositions from selected anhydrous experiments saturated in ol, ol + plg and ol + plg + cpx at 1 bar from *Grove and Bryan* [1983], *Grove et al.* [1990], *Yang et al.* [1996], and P. Ulmer (unpublished data, 2004). Lines connecting data points denote liquid lines of descent of different starting compositions (plg in, solid; cpx in, dashed). Within the gray shaded area, liquids of low-pressure experiments not saturated in cpx could overlap with high-pressure liquids.

and Cornell [1998] inverted these models to calculate crystallization pressures and compared them with numerical models of *Danyushevsky et al.* [1996] and *Weaver and Langmuir* [1990]. *LeRoux et al.* [2002] applied this approach to the southern Mid-Atlantic Ridge (40°–55°N). *Herzberg* [2004] parameterized the ol-cpx-plg saturation planes of anhydrous experiments on basalts for a different projection and applied the calculated crystallization pressures to a large database of MORB glasses. All of these studies came to similar conclusions. Mid-ocean ridge basalts crystallize at the ocean floor and within the underlying mantle at depths up to 30 km (1.0 GPa). The available models to calculate crystallization pressures of tholeiitic liquids are calibrated with glass compositions from near-liquidus equilibrium crystallization experiments. However, the compositional variation along the liquid line of descent of tholeiitic basalts is limited, particularly at high pressure.

[4] In this paper we present a simple liquid composition barometer based on the evolution of CaO with decreasing Mg # [= Mg/(Mg + Fe), all Fe as Fe^{2+}]. The barometer is calibrated against glass compositions saturated in cpx and plg (± ol, opx, spi) from equilibrium crystallization experiments at pressures of 1 bar to 1.0 GPa (for references, see Figure 1). Including liquid compositions from fractional crystallization experiments at 1.0 GPa [*Villiger et al.*, 2004] permits us to calibrate the barometer over a large compositional range along the liquid line of descent of anhydrous basalts.

[5] We discuss the effects of variable starting materials and H_2O content with respect to the evolution of CaO versus Mg # during differentiation of mafic magmas. We compare our barometer with previous calibrations to calculate crystallization pressures [e.g., *Grove et al.*, 1992; *Yang et al.*, 1996; *Herzberg*, 2004]. We find that our new calibration is comparable to previous formulations at low pressure, while at high pressure it provides substantially better reproduction of the experimental data set, mainly as a result of including compositions fractionated at high pressures. Finally, we apply the new barometer to a large data set of MORB glasses (derived from Petrological Database of the Ocean Floor: http://www.petdb.org) and discuss the influence of pressure on the diversity of MORB from three different mid-ocean ridges (East Pacific Rise, Mid-Atlantic Ridge, Southwest Indian Ridge).

[6] The statistical distribution of calculated crystallization pressures for these ridge systems correlates with spreading rate, once the data set has been corrected for hot spot-influenced areas. Our new liquid barometer thus permits us to quantify the average crystallization depth of mafic magmas at individual spreading centers. These calculations are discussed in the light of recent drilling results from mid-ocean ridges and support the hypothesis that crystallization of basaltic liquids at upper mantle pressures is an important

process that has to be taken into account for realistic models of the composition of the oceanic crust.

2. Melt Composition Barometer

2.1. Development of a New Equation for Pressure Calculations

[7] Liquid compositions of primitive mid-ocean ridge basalts calculated with numerical and thermodynamic models (*Weaver and Langmuir* [1990]; MELTS, *Ghiorso and Sack* [1995] and *Ghiorso et al.* [2002]; PETROLOG, *Danyushevsky et al.* [1996]; COMAGMAT, *Ariskin* [1999] and *Ariskin et al.* [1993]) and glass compositions from fractional and equilibrium crystallization experiments [*Villiger et al.*, 2004, 2007] show a positive correlation of CaO with temperature, MgO or Mg #, if the magma is not saturated in plagioclase or cpx. The CaO maximum along the liquid lines of descent of anhydrous basaltic magmas is systematically higher at low pressure than at high pressure, mainly because of the expansion of the olivine primary phase field at low pressure [*Bowen*, 1928; *Kushiro*, 1969]. After the crystallization of cpx the CaO liquid lines of descent decrease at various pressures with a similar slope. This is illustrated in Figure 1a, showing the covariance of CaO against Mg # of selected experimental glass compositions at pressures between 1 bar and 1.0 GPa. Different Clapeyron slopes for olivine saturation with respect to the saturation of cpx broaden the stability field of olivine toward lower pressures (see discussion by *Villiger et al.* [2007]).

[8] The slopes and intercepts of equation (1) were obtained by multiple least squares regression of glass compositions of selected experimental data sets (for references, see Figure 1), which were saturated in plg, cpx (± ol, opx and spi) at pressures of 1 bar, 0.2 GPa, 0.8 GPa and 1.0 GPa. Experimental data used to obtain the fit are limited to olivine-saturated compositions at the pressure of cpx-plg saturation, or lie on the liquid line of descent of such experiments. If this criterion is violated, slopes in a CaO versus Mg # diagram of glass compositions of experiments performed at high pressures and with starting materials without olivine as a liquidus phase could lie on liquid lines of descent corresponding to lower pressures. The straight lines in Figure 1a are calculated isobars for pressures between 1 bar and 1.0 GPa. The slopes and intercepts for the calculated pressures are listed in Figure 1a.

$$\mathrm{CaO\,(wt\%)} = 3.98(\pm0.17) + 14.96(\pm0.34) \times \mathrm{Mg\ \#\ (molar)]} \\ -0.260(\pm0.008)]P(\mathrm{kbar}),\ r^2 = 0.92 \qquad (1)$$

To calculate crystallization pressures of cpx-plg saturated tholeiitic magmas, equation (1) was converted into

$$P(\mathrm{kbar}) = [\mathrm{CaO\,(wt\%)} - 3.98(\pm0.17) - 14.96(\pm0.34) \\ \times \mathrm{Mg\ \#\ (molar)}]/[-0.260(\pm0.008)],\ r^2 = 0.92 \qquad (2)$$

2.2. Analytical Uncertainties and Compositional Restrictions

[9] CaO contents of glasses from selected experimental studies at 1 bar using different starting compositions are plotted against Mg # in Figure 1b. They include experiments saturated in ol, ol + plg and ol + plg + cpx separated by phase boundaries (cpx-in and plg-in). The cpx-in line is parallel to the 1 bar CaO versus Mg # trend, clearly indicating that the barometer is only valid for cpx-saturated liquids. Glass compositions of 1 bar experiments reach the fitted cpx-plg-ol line by fractionation of dunitic (ol) or troctolitic (ol + plg) residues starting from compositions with different Mg # (0.58 to 0.76, for references, see Figure 1b). The gray shaded area marks the range of compositions where low-pressure liquids saturated in olivine only, or olivine and plagioclase may overlap with high-pressure liquids saturated in cpx and plagioclase. Thus applying our barometer to primitive tholeiitic liquids with Mg # > 0.6 substantially overestimates calculated crystallization pressures.

[10] The calculated pressures are sensitive to both within-lab and interlaboratory uncertainties of analytical data, as discussed in detail by *Michael and Cornell* [1998]. For example, if we use the 2σ errors of 1.0 GPa experimental glass compositions [*Villiger et al.*, 2004], the calculated pressure uncertainty is $\sim\pm$ 0.1 GPa (Figure 1a), similar to uncertainty estimates by *Grove et al.* [1992]. Different analyses of the same basalt glasses, measured in different laboratories, were obtained from the PETDB database to constrain the sensitivity of our barometer to interlaboratory uncertainties. We find that results for most of the glasses are within 0.1 GPa, although in some cases, pressure differences exceeding 0.1 GPa were calculated.

2.3. Validation and Accuracy of the Barometer

[11] To test the reliability of the CaO/Mg # barometer, calculated pressures of experimental glasses, which have been used for the calibration, are plotted against experimental pressures in Figure 2a. The same data set has been used to calculate pressures with the expression of *Herzberg* [2004] (Figure 2b) and the inversion of the models of *Grove et al.* [1992] (Figure 2c) and *Yang et al.* [1996] (Figure 2d). *Herzberg* [2004] converted liquid compositions into normative enstatite, diopside and anorthite. Experimental glasses saturated with ol, plg and cpx define isobars in the anorthite-diopside-enstatite plane and were used to derive an expression to calculate crystallization pressures. Applying the method of *Grove et al.* [1992], pressure was calculated by averaging pressures calculated from four different equations using normative ol, cpx, plg and qtz compositions of the melts, respectively. *Yang et al.* [1996] recalculated liquid compositions in wt % to molar fractions and fitted equations for X_{Ca}, Mg # and X_{Al} as a function of pressure and liquid compositions expressed as X_{Na}, X_K, X_{Si}, X_{Ti} and X_{Fe}. We calculated crystallization pressures for multiply saturated liquids (ol, cpx and plagioclase) by applying the inverted equation for X_{Ca}, which is least dependent on analytical errors. The results of pressure calculations are listed in Table 1 and graphically shown in Figure 2c.

[12] Averages of calculated pressures against corresponding experimental pressures and statistical parameters are listed in Table 1 and graphically shown in Figure 2. The crystallization pressures calculated with the methods of *Herzberg* [2004] and *Grove et al.* [1992] underestimate pressures at 0.8 GPa and fractional crystallization experiments at 1.0 GPa. The method of *Yang et al.* [1996] appears to reproduce the experimental pressures best. All of these methods fail in

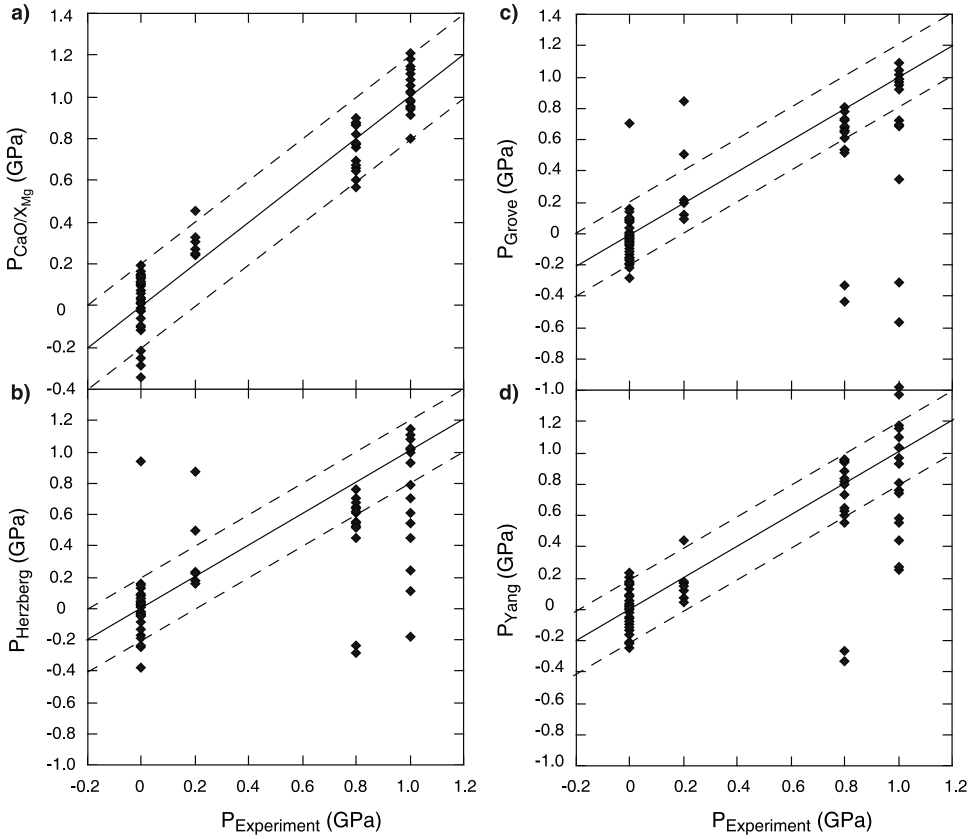

Figure 2. Calculated pressures plotted against experimental pressures of selected anhydrous experiments saturated in cpx (±plg, ol, opx, spi) used for the calibration of the CaO–Mg # barometer. (a) Pressure calculated with equation (2) using CaO in wt % and Mg #. (b) Pressures calculated with the equation of *Herzberg* [2004]. (c) Pressures calculated using the average pressures of the inverted equations from *Grove et al.* [1992]. (d) Pressures calculated using the inverted equation for X_{Ca} from *Yang et al.* [1996]. Sources of data are as in Figure 1.

calculating crystallization pressures for glasses from fractional crystallization experiments at 1.0 GPa and equilibrium crystallization experiments at 0.8 GPa with differentiated compositions (Mg # = 0.24, 0.26 [*Baker and Eggler*, 1987]). Including primitive to differentiated glass compositions from fractional crystallization experiments (Mg # 0.67–0.12) in the calibration of our barometer permits us to calculate pressures of differentiated basalts that are saturated in cpx and plg (±ol and spi).

2.4. Effect of H_2O on the CaO/Mg # Barometer

[13] To test the influence of H_2O on the CaO/Mg # barometer in basaltic systems, we evaluated a number of H_2O undersaturated and H_2O saturated experimental liquid compositions (Figure 3a). *Sisson and Grove* [1993] and *Berndt et al.* [2005] explored the effects of H_2O on basaltic bulk compositions. The prolonged crystallization of olivine drives the CaO content of derivative liquids to higher values than the corresponding anhydrous 0.2 GPa isobar would indicate. The CaO/Mg # ratio in H_2O saturated experiments is controlled by a higher cpx/plg ratio, a slightly higher CaO content of cpx, and in particular by higher anorthite contents of plagioclase with respect to anhydrous experiments, resulting in a steeper slope of isobars in the CaO/Mg # diagram compared to anhydrous experiments. Water undersaturated experiments with MORB-like bulk compositions

Table 1. Compilation of Averages and Standard Deviations of Calculated Crystallization Pressures (P_{cal}) Determined With Various Methods According to the Pressures (P_{epx}) of Experiments Used for the Calibration of the CaO/Mg # Barometer[a]

				P_{cal}, GPa		$P_{cal} - P_{exp}$	
Barometer	Reference	N	P_{exp}, GPa	Average	SD	y	r^2
Ca/Mg #	this study	36	0.001	0.02	0.14	1	0.92
		7	0.2	0.3	0.08		
		15	0.8	0.75	0.11		
		17	1	1.03	0.11		
ol-cpx-plg-qtz	*Grove et al.* [1992]	36	0.001	−0.02	0.17	0.7	0.52
		7	0.2	0.31	0.27		
		15	0.8	0.52	0.38		
		17	1	0.6	0.62		
an-di-en	*Herzberg* [2004]	36	0.001	0.01	0.2	0.63	0.36
		7	0.2	0.33	0.26		
		15	0.8	0.48	0.31		
		17	1	0.74	0.39		
X_{ca}	*Yang et al.* [1996]	36	0.001	0.01	0.14	0.81	0.67
		7	0.2	0.17	0.13		
		15	0.8	0.75	0.4		
		17	1	0.82	0.32		

[a] N is the number of experimental glasses at each pressure. $P_{cal} - P_{exp}$ shows the parameters (y, slope; r^2, residuals squared) of linear regression between experimental and calculated pressures.

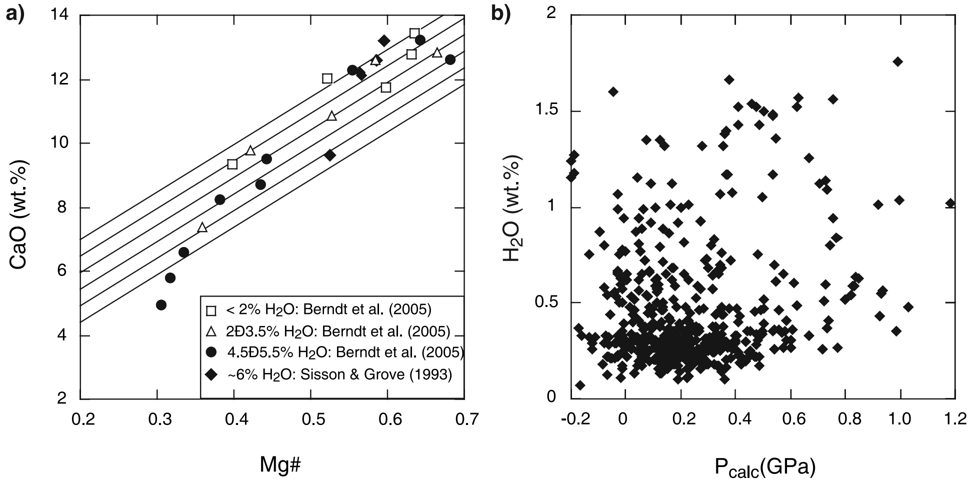

Figure 3. (a) CaO in wt % hydrous experimental glasses with variable H_2O content (e.g., <2.0; 2.0–3.5; 4.5–5.5; 6 wt %) at 0.2 GPa from *Sisson and Grove* [1993] and *Berndt et al.* [2005] plotted against Mg #. (b) H_2O (wt %) content of glasses from mid-ocean ridges of the Atlantic, Indian, and Pacific oceans as well as from back-arc basins with Mg # <0.6 plotted against calculated pressure using the CaO–Mg # barometer. Major element and H_2O contents of the glasses are from the PETDB database (http://www.petdb.org). Glass analyses are normalized to 100% anhydrous compositions.

are rare. Experimental glass compositions at 0.2 GPa from *Berndt et al.* [2005] with H_2O contents below 2 wt % scatter between the 1 bar and 0.4 GPa isobars. The glasses with higher H_2O contents (2–3.5 wt %) show no clear correlation either. In addition, glass compositions from mid-ocean ridges with measured H_2O contents are plotted in Figure 3. They do not show a correlation between H_2O content and calculated pressure. From these observations and from the experimental constraints, we infer that small amounts of water (<1 wt %) relevant for MORB will not significantly affect the calculated pressures.

3. Chemical Variability of Experimental Glass Compositions

[14] In order to assess the compositional variability of natural MORB glasses with respect to fractionation processes at variable pressure, we have first plotted variation diagrams of glass compositions derived from fractional and equilibrium crystallization experiments between 1 bar and 1.0 GPa (Figure 4). Here we summarize the most important results with respect to MORB evolution. For a more detailed discussion of melt compositional variability, see *Villiger et al.* [2007].

[15] For fractional crystallization experiments at 1.0 GPa, SiO_2 evolves through continuous enrichment from basaltic to rhyodacitic compositions [*Villiger et al.*, 2004]. At 0.7 GPa, SiO_2 increases moderately along the liquid line of descent up to ilmenite saturation, where a strong increase can be observed [*Villiger et al.*, 2007]. The equilibrium crystallization experiments at 1 bar, 0.2 GPa and 0.8 GPa evolve through constant SiO_2 (48–53 wt %) except for two experiments at 0.8 GPa, with 57.1 and 57.8 wt % SiO_2, respectively. The different behavior of SiO_2 is dependent on (1) the degree of melting and (2) the pressure of melting. At constant pressure, SiO_2 generally decreases with increasing melt fractions [*Falloon and Green*, 1987, 1988; *Baker et al.*, 1995]. With increasing pressure, the multiple saturation point moves toward the olivine apex, thus decreasing the SiO_2 content of the equilibrium liquid [e.g., *Ulmer*, 2001].

[16] The maximum Al_2O_3 content of dry experimental liquids is mainly controlled by plagioclase saturation, which in turn is controlled by the bulk composition, crystallization pressure and melt H_2O content (Figure 4c). For fractional crystallization experiments, liquids reach the maximum Al_2O_3 content at 1.0 GPa (17.8 wt %, at 5.9 wt % MgO). In contrast, experimental data at 1 bar suggest that the maximum Al_2O_3 content does not exceed 14.5 wt %. Al_2O_3 contents of experimental glasses at 1 bar, 0.2 GPa and 0.8 GPa, used for calibration of the CaO/Mg # barometer, display a larger scatter, which mainly depends on the pressure and the extent of melting, and the composition of the mantle source for individual data sets. For a given melt fraction, melts extracted from the mantle at high pressures are lower in Al_2O_3 than melts produced at low pressures [*Hirschmann et al.*, 1998, 1999; *Kushiro*, 2001]. On the other hand, enhanced olivine and cpx fractionation at high pressure leads to an enrichment of Al_2O_3 with decreasing Mg # at 0.7 and 1.0 GPa. FeO (all Fe as Fe^{2+}) enrichment during crystallization is subdued at 1.0 GPa compared to 0.7 GPa or at 1 bar (Figure 4d), and different for fractional versus equilibrium crystallization [*Villiger et al.*, 2007]. At 0.7 GPa, FeO reaches a maximum in the liquid of 16.5 wt %, versus <10 wt % at 1.0 GPa, decreasing with subsequent ilmenite crystallization. Liquids derived from equilibrium crystallization experiments at 0.7 to 1.0 GPa reach lower FeO maxima than the ones from fractional crystallization. Some of the equilibrium crystallization experiments at 0.2, 0.8 and 1.0 GPa with higher FeO at the same Mg # as the fractional crystallization experiments evolve along the 1 bar trend. This is primarily due to suppressed crystallization of Fe-Ti oxides in closed-system equilibrium experiments. Additional factors controlling the FeO content of basaltic liquids, such as pressure and extent of melting, have been discussed extensively [e.g., *Langmuir et al.*, 1992]. Na_2O moderately increases with fractionation, reaching a ‘plateau’

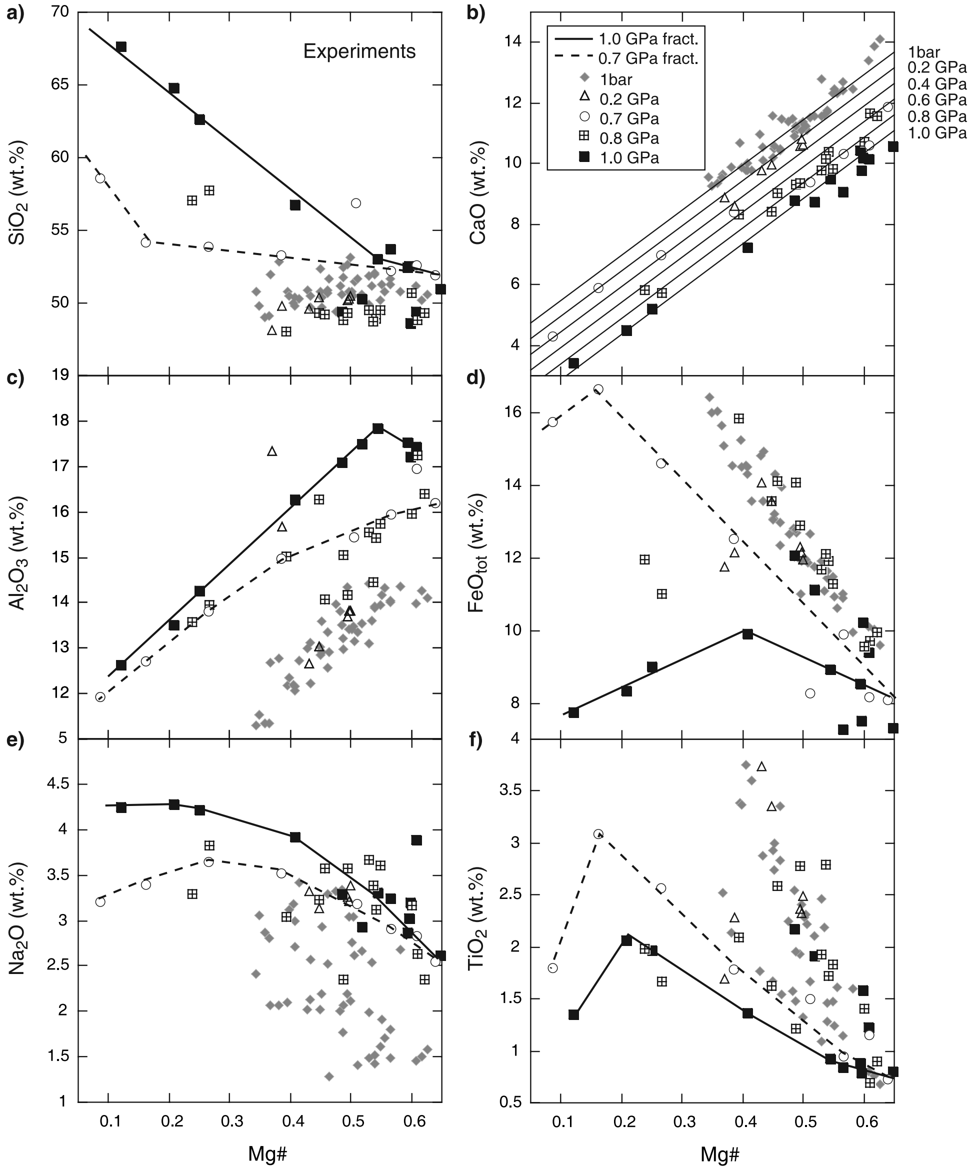

Figure 4. Variation diagrams of (a) SiO_2, (b) CaO, (c) Al_2O_3, (d) FeO_{tot} (all Fe as Fe^{2+}), (e) Na_2O, and (f) TiO_2 in wt % plotted against Mg # from glasses of anhydrous experiments (normalized to 100%). 1 bar experiments, gray diamonds; 0.2 GPa, open triangles; 0.7 GPa, open circles; 0.8 GPa, boxes with cross; 1.0 GPa, solid squares. Sources of data are as in Figure 1. The lines mark the compositional liquid lines of descent of fractional crystallization experiments at 0.7 GPa (dashed line) from *Villiger et al.* [2007] and 1.0 GPa (straight line) from *Villiger et al.* [2004].

at 1.0 GPa and a maximum at 0.7 GPa, respectively. The weak decrease at low Mg # in the experimental series at 0.7 GPa [*Villiger et al.*, 2007] indicates increasing cotectic proportions of plg relative to cpx at lower pressures. However, there is a large spread in Na_2O at a given Mg # for most of the 1bar experiments, which derives in part from experimental uncertainties associated with Na loss and in part indicates that the primary control on Na_2O in many experimental studies is the initial Na_2O content of the liquid, which primarily depends on the degree of melting [e.g., *Klein and Langmuir*, 1987; *Baker et al.*, 1995]. Liquid TiO_2 content behaves similarly to FeO. For fractional crystallization experiments at 0.7 GPa and 1.0 GPa, a moderate increase in TiO_2 is recorded until the crystallization of ilmenite (Figure 4f). At a given Mg #, the TiO_2 increase is more pronounced in liquids crystallized at 0.7 GPa than at 1.0 GPa. Equilibrium crystallization experiments with different bulk compositions at 1 bar, 0.2 GPa, 0.8 GPa and 1.0 GPa follow different TiO_2 trends; the highest TiO_2 values at a given Mg # are observed at low pressure.

4. Application of the CaO/Mg # Barometer to Mid-ocean Ridge Basalts

[17] The new CaO/Mg # barometer has been applied to a variety of mid-ocean ridge basalts from localities with different spreading rates. We have selected an example of a fast spreading ridge (East Pacific Rise (EPR)), a slow

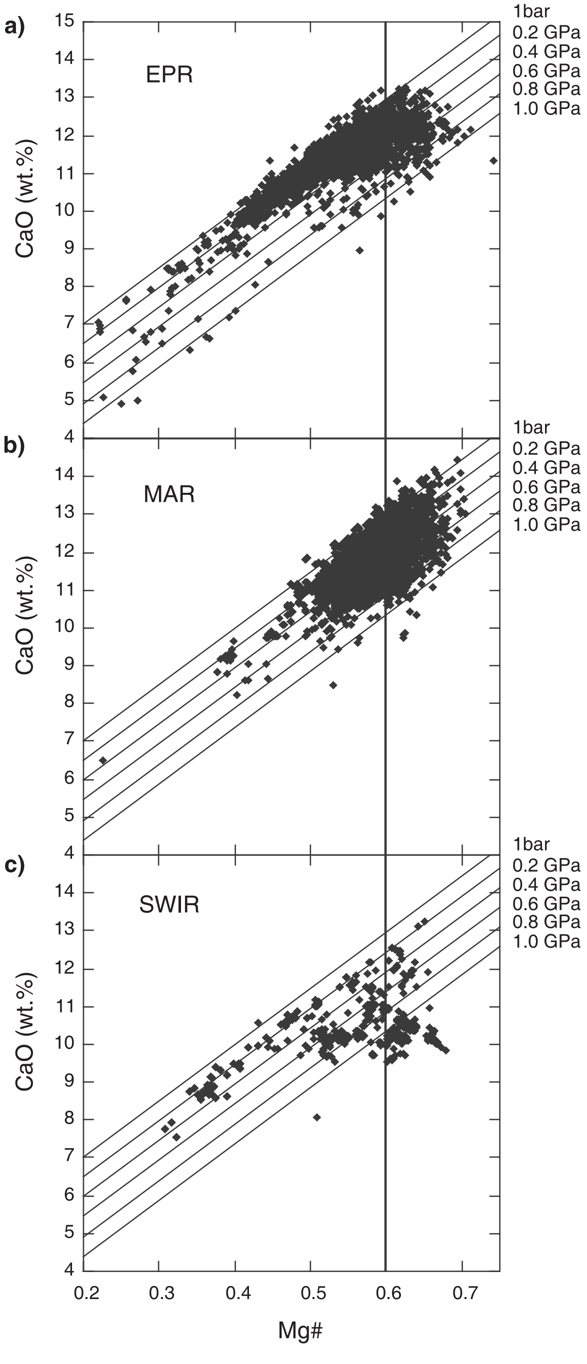

Figure 5. CaO in wt % of glasses (normalized to 100%) from (a) the East Pacific Rise (EPR), (b) the Mid-Atlantic Ridge (MAR), and (c) the Southwest Indian Ridge (SWIR) plotted against Mg #.

spreading ridge (Mid-Atlantic Ridge (MAR)) and an ultra-slow spreading ridge (Southwest Indian Ridge (SWIR)). For the slow spreading ridges we accounted for possible influences of mantle plumes (Figure 5). The K_2O/TiO_2 ratio has been taken as indicator for hot spot-affected ridge segments. All glass analyses taken from the PETDB database covering the whole range of Mg # have been normalized to 100% anhydrous and plotted on the CaO/Mg # variation diagrams. Overall, the three different ridges show a wide variety of equilibration pressures between near-surface conditions up to pressures exceeding 1.0 GPa. One aspect of plotting a large number of data in these diagrams is that primitive glasses with Mg # > 0.6 show generally higher crystallization pressures than more evolved glasses. A second important observation is that extremely fractionated basalts with Mg # <0.4 mainly occur at the fast spreading EPR, whereas there is virtually no ferrobasalt at the slower spreading MAR and SWIR, except in areas that are influenced by hot spot magmatism. Thus a stratification of the oceanic crust, with Mg-rich mafic rocks in the lower crust and more Fe-rich mafic rocks in the upper crust, as, for example, in the Oman ophiolite [*Pallister and Hopson*, 1981; *Kelemen et al.*, 1997], is likely to be developed at the fast spreading EPR but cannot conclusively be deduced from the MAR and the SWIR data. The statistically significant difference in crystallization pressure between the three ridge systems is further illustrated in Figure 6. Histograms of calculated pressures for EPR (Figure 6a), MAR (Figure 6b) and SWIR (Figure 6c) glasses (Mg # < 0.6) demonstrate the statistical distribution of fractionation depths below different mid-ocean ridges. At a given Mg #, crystallization pressures are substantially different. For example, calculated pressures for basalts with restricted Mg # (0.545 < Mg # < 0.555) with no hot spot influence (see below) vary from ~0.2 GPa for the EPR (n = 170), to 0.45 GPa for the MAR (n = 298) to 0.64 GPa for the SWIR (n = 11). Taken together, these calculations suggest a reasonable correlation of the depth of basalt fractionation with spreading rate and the thickness of the lithosphere on axis. In the following, we explore in more detail the regional variability of calculated pressures, by plotting along-axis variations for each of the three regions.

4.1. East Pacific Rise (25°S–25°N)

[18] The average crystallization pressure for glasses of the EPR between 25°S and 25°N is 0.20 ± 0.15 GPa (Figure 7). Pressures below 0.25 GPa are calculated for 77.9% of all glasses; 20.5% of the calculated pressures lie within 0.25 to 0.6 GPa and only 1.6% of the EPR glasses show pressures higher than 0.6 GPa. Most of the glasses with pressures higher than 0.25 GPa are concentrated on the section of ridge between 8°N and 15°N and at fracture zones. Pressures higher than 0.6 GPa are observed for the ridge segment between 8°N and 15°N. Within this portion of the ridge the highest pressures have been calculated for the Siqueiros Fracture Zone (P < 1.2 GPa) and the ridge segment between 11°N and 13°N, which is associated with the termination of spreading centers and deviations from axial linearity [*Langmuir et al.*, 1986; *Reynolds et al.*, 1992; *Macdonald et al.*, 1988]. In contrast, pressures below ~0.3 GPa have been calculated for glasses from the Clipperton Fracture Zone (10°30'N). Tectonic reconstructions by *Pockalny et al.* [1997] using bathymetry, side scan and magnetic data indicate periods of oblique spreading along the Cocos Plate over the last 2.5 Ma, which caused a series of compressional events along the Clipperton Fracture Zone and a series of extensional events along the Siqueiros Fracture Zone. The transpressional regime at the Clipperton Fracture Zone offers a possible explanation for the lack of elevated crystallization depths for the Clipperton glasses relative to a transtensional regime at the Siqueiros Fracture Zone. A transtensional regime is also described at the Garrett Trans-

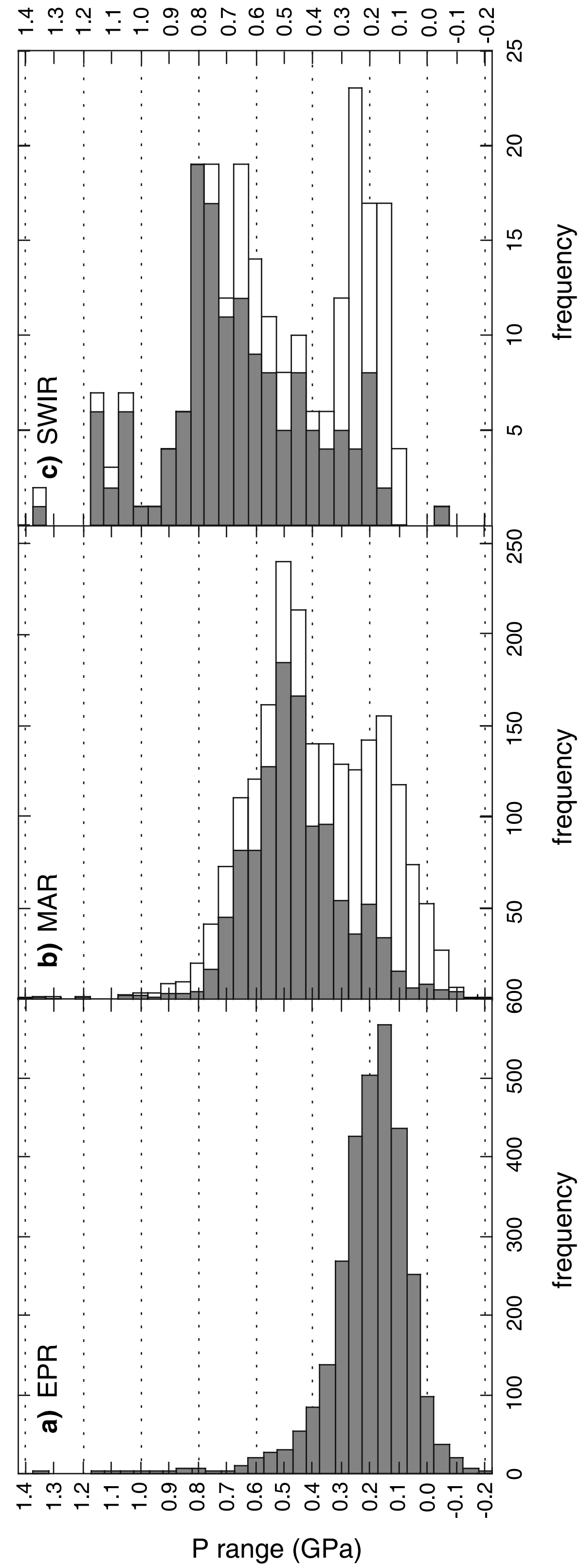

Figure 6. Histograms of calculated pressures for glasses of basalts from (a) the East Pacific Rise (EPR), (b) the Mid-Atlantic Ridge (MAR), and (c) the Southwest Indian Ridge (SWIR). For pressure calculations with the CaO–Mg # barometer only glass analyses normalized to 100% with Mg # < 0.6 were used. Gray shaded histograms contain data of normal ridge segments that are not affected by hot spots.

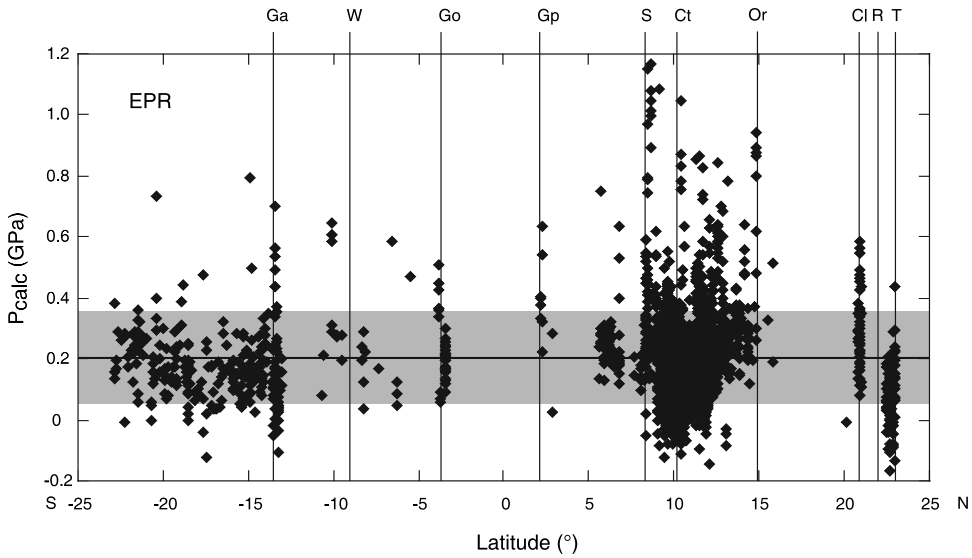

Figure 7. Calculated pressures for glasses of basalts from the East Pacific Rise (EPR) between 25°S and 25°N plotted against latitude. For pressure calculations with the CaO–Mg # barometer, glass analyses have been normalized to 100% and glasses with Mg # < 0.6 were used. The horizontal line represents the average pressure of 0.20 GPa from 3017 glasses. The gray shaded area defines their standard deviation of ±0.15 GPa. Vertical lines mark the positions of fracture zones (FZ): Ga, Garrett; W, Wilkes; Go, Gofar; Gp, Galapagos; S, Siqueiros; Ct, Clipperton; Or, Orozco; Cl, Clarion; R, Rivera; T, Tamayo.

form fault, which developed three small ridges, named the Alpha, Beta and Gamma ridges [e.g., *Niu and Hékinian*, 1997; *Wendt et al.*, 1999]. At both fracture zones primitive lavas are described (Siqueiros, *Perfit et al.* [1996]; Garrett, *Wendt et al.* [1999]) and interpreted as primitive liquids with little or no fractionation in shallow crustal reservoirs.

[19] Major element variations in EPR glasses are plotted against Mg # (Figure 8). We grouped the analyzed glasses somewhat arbitrarily into three classes of (1) calculated crystallization pressures below 0.25 GPa, (2) pressures between 0.4 and 0.6 GPa, and (3) pressures above 0.75 GPa. The vast majority of low-pressure EPR glasses evolve with constant SiO_2, only at Mg # < 0.3 does SiO_2 increase moderately. Combined with decreasing FeO and TiO_2 contents at similar Mg #, late stage SiO_2 increase is probably related to the fractionation of Ti-Fe bearing phases (ilmenite and/or titano-magnetite). Glass compositions with estimated crystallization pressures > 0.75 GPa follow the trend of the 1.0 GPa glasses evolving through continuous SiO_2 increase to rhyodacitic compositions. Data for the glasses that crystallized between 0.4 and 0.6 GPa plot between values for high-pressure and low-pressure glasses.

[20] For a given Mg # of ~0.6, the low-pressure liquid line of descent of Al_2O_3 scatters by about 2 wt %, which probably reflects variable depths and degree of mantle melting [*Kushiro*, 2001]. However, we argue that data for the glasses with crystallization pressures > 0.75 GPa plot at higher Al_2O_3 contents than the low-pressure ones though they plot below the experimental 1.0 GPa liquid line of descent (Figure 8c).

[21] FeO of most low-pressure melts evolve with the steepest slope, following the 1 bar trend. Liquids fractionating at the highest pressures display a less pronounced increase of FeO but are always higher than the experimental 1.0 GPa liquid line of descent. Some of the glasses with intermediate crystallization pressures plot in between the high- and the low-pressure trends and some plot along the average of the 1 bar trend, probably reflecting the predominance of fractional or equilibrium crystallization, respectively. As discussed above, the FeO content of derivative liquids depends on the FeO content of the primary liquid, which itself is dependent on the mean pressure of melting [*Klein and Langmuir*, 1987; *Langmuir et al.*, 1992].

[22] The variability of the Na_2O content of EPR glasses at calculated pressures <0.25 GPa probably reflects variable degrees of melting for different lava suites. However, Na_2O is displaced toward higher values at a given Mg # for samples with increasing pressure of crystallization.

[23] TiO_2 contents range from ~1 wt % up to 3.6 wt % (Figure 8f), but mostly cluster along the low-pressure liquid line of descent and only a few evolved samples exhibit a relative decrease at Mg # < ~0.3. The fractionation trends at high pressures loosely follow the experimentally determined liquid lines of descent, albeit at somewhat lower pressures.

[24] Data for glasses from the Siqueiros Fracture Zone exhibit crystallization pressures exceeding 0.75 GPa and show calculated Na_8 (defined after *Klein and Langmuir* [1987]) between 2.8 and 3.2 wt %, which is significantly higher than low-pressure glasses with Na_8 values ranging from 2.2 to 2.8 wt %. They also have higher values in incompatible elements like TiO_2, Na_2O and K_2O at similar Mg #, which has been ascribed to a transform fault effect [*Bender et al.*, 1984; *Langmuir and Bender*, 1984]. On the basis of Zr/Y ratios of glasses from the Siqueiros Fracture Zone, *Perfit et al.* [1996] modeled the extent of peridotite melting. Both major element compositions and Zr/Y ratios

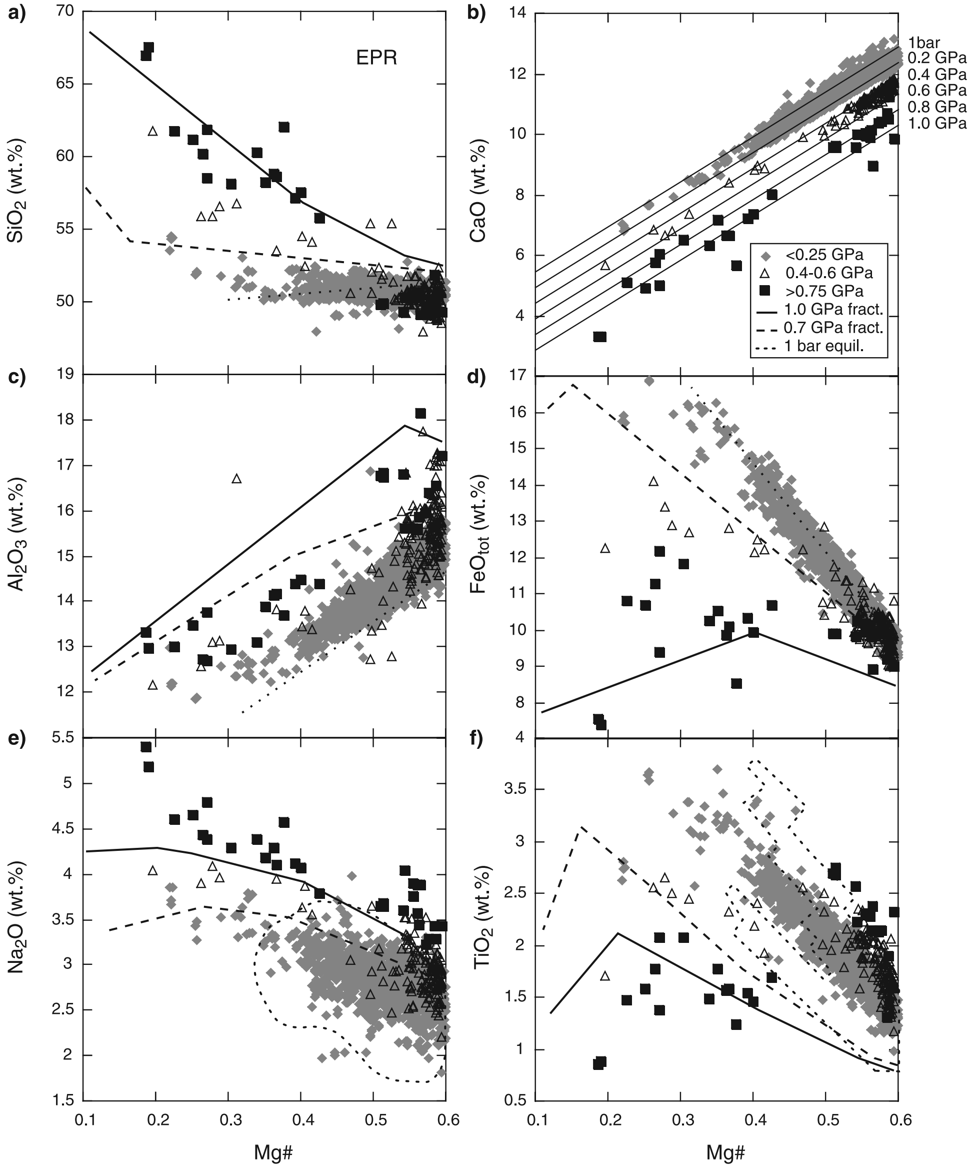

Figure 8. Variation diagrams of (a) SiO_2, (b) CaO, (c) Al_2O_3, (d) FeO_{tot}, (e) Na_2O, and (f) TiO_2 in wt % plotted against Mg # for glasses of the East Pacific Rise (EPR). Glass compositions are grouped into three classes of calculated crystallization pressures. Pressure < 0.25 GPa, gray diamonds; pressure 0.4–0.6 GPa, open triangles; pressure >0.75 GPa, black squares. Lines mark the liquid lines of descent of fractional crystallization experiments at 0.7 GPa (dashed line) and at 1.0 GPa (straight line). Small dashes indicate the average of experimental glasses at 1 bar.

of the glasses with the highest crystallization pressures are consistent with a liquid derived from a low degree of partial melting followed by high-pressure fractional crystallization.

4.2. Mid-Atlantic Ridge (55°S–52°N)

[25] Estimated pressures for MAR glasses (Mg # < 0.6) between 55°S and 52°N result in a bimodal distribution with a peak around 0.2 GPa and another around 0.5 GPa (Figure 6b). The average pressure for the whole data set of 2110 analyses is 0.38 ± 0.21 GPa. For a segmented mid-ocean ridge with a lower spreading rate, a higher average crystallization pressure is predicted because the thermal lithosphere is likely to be thicker than at fast spreading ridges [e.g., *Ghose et al.*, 1996].

[26] Mantle heterogeneities and hot spot ridge interaction were first described for the MAR by *Schilling* [1975]. According to *Shen and Forsyth* [1995] K_2O/TiO_2 is a good indicator for an incompatible-element-enriched mantle source. It can be correlated with anomalies of trace element ratios (e.g., La/Sm, Nb/Zr), isotope systematics (e.g., Sr, Nd, Pb, U-Th, He, and Hf isotopic systems), as well as bathymetric and geophysical data (axial depth, crustal thickness, gravity and seismic tomography). Therefore we plotted K_2O/TiO_2 ratios of the MAR glasses against latitude, together with locations of hot spots (Figure 9b). K_2O/TiO_2 ratios > 0.2 were taken as a proxy for ridge–hot spot interactions, and are found all along the MAR, including some locations far away from any known hot spot.

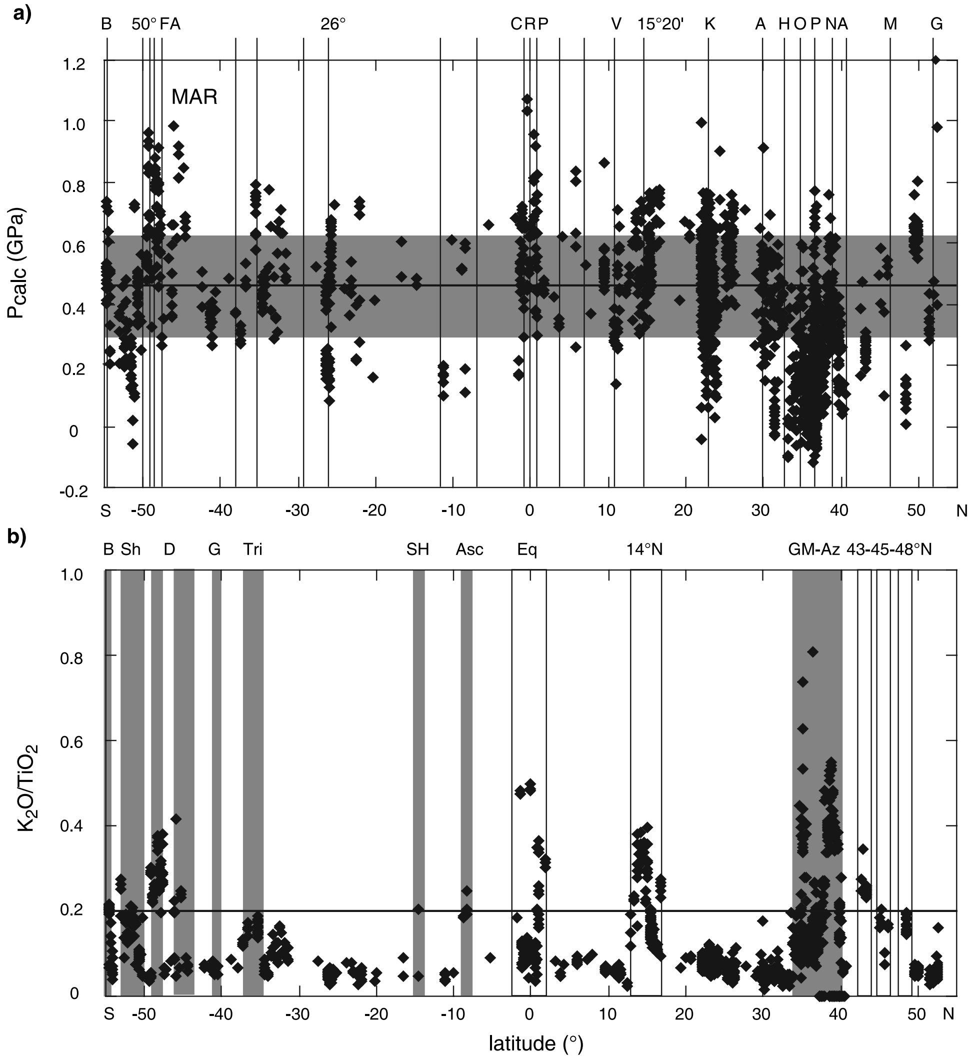

Figure 9. (a) Calculated pressures for glasses of basalts from the Mid-Atlantic Ridge (MAR) between 55°S and 52°N plotted against latitude. For pressure calculations with the CaO–Mg # barometer, glass analyses have been normalized to 100%, and glasses with Mg # < 0.6 were used. The horizontal line represents the average pressure of 0.46 GPa of 1126 glasses of MAR segments possibly not affected by hot spots. The gray shaded area defines their standard deviation of ±0.17 GPa. Vertical lines mark the positions of fracture zones (FZ): B, Bouvet; 50°, 50°; FA, Falkland–Agulhas; 26°, 26°S; C, Chain; R, Romanche; P, St. Paul; V, Vema; 15°20′, 15°20′N; K: Kane; A, Atlantis; H, Hayes; O, Oceanographer; P, Pico; NA, North Azores; M, Maxwell; G, Gibbs. (b) K_2O/TiO_2 ratios of glasses plotted against latitude. Horizontal black line marks a K_2O/TiO_2 ratio of 0.2. Gray vertical boxes indicate regions of possibly hot spot-influenced ridge sections. B, Bouvet; Sh, Shona; D, Discovery; G, Gough; Tri, Tristan da Cunha; SH, St. Helena; Asc, Ascension; Az, Azores hot spots. White boxes, additional ridge segments with K-enriched basalts (e.g., Eq (equatorial region), 14°N, 43°N, 45°N, and 48°N anomalies).

[27] Crystallization pressures below 0.3 GPa preferentially occur along ridge segments influenced by mantle plumes like the Bouvet hot spot between 55° and 50°S, at the Jussieu-Azores Platform between 33° and 40°N as well as at 43° and 48° N. For "normal" ridge segments, low crystallization pressures are observed from the Kane and the 26°S Fracture Zones, respectively. Crystallization pressures exceeding 0.7 GPa are obtained for glasses from fracture zones at "normal" as well as hot spot-influenced ridge segments (Figure 9b). Crustal magma chambers have been seismically imaged below the Reykjanes Ridge [*Navin et al.*, 1998].

[28] When we eliminate glass analyses from MAR segments that are possibly affected by hot spots, the bimodal distribution disappears (Figure 6b). The remaining 1126 glasses from "normal" MAR segments plot around an average pressure of 0.46 ± 0.17 GPa. Glasses crystallized at pressures <0.25 GPa represent 14.2% of the data set, 82.9% lie between 0.3 to 0.7 GPa and about 2.9% of the glasses show pressures higher than 0.7 GPa.

[29] Selected oxides of MAR glasses grouped by calculated crystallization pressures ($P < 0.25$ GPa, $P = 0.4–0.6$ GPa, $P > 0.75$ GPa) are plotted against Mg # < 0.6 (Figure 10b). The MAR glasses do not show well-defined trends and,

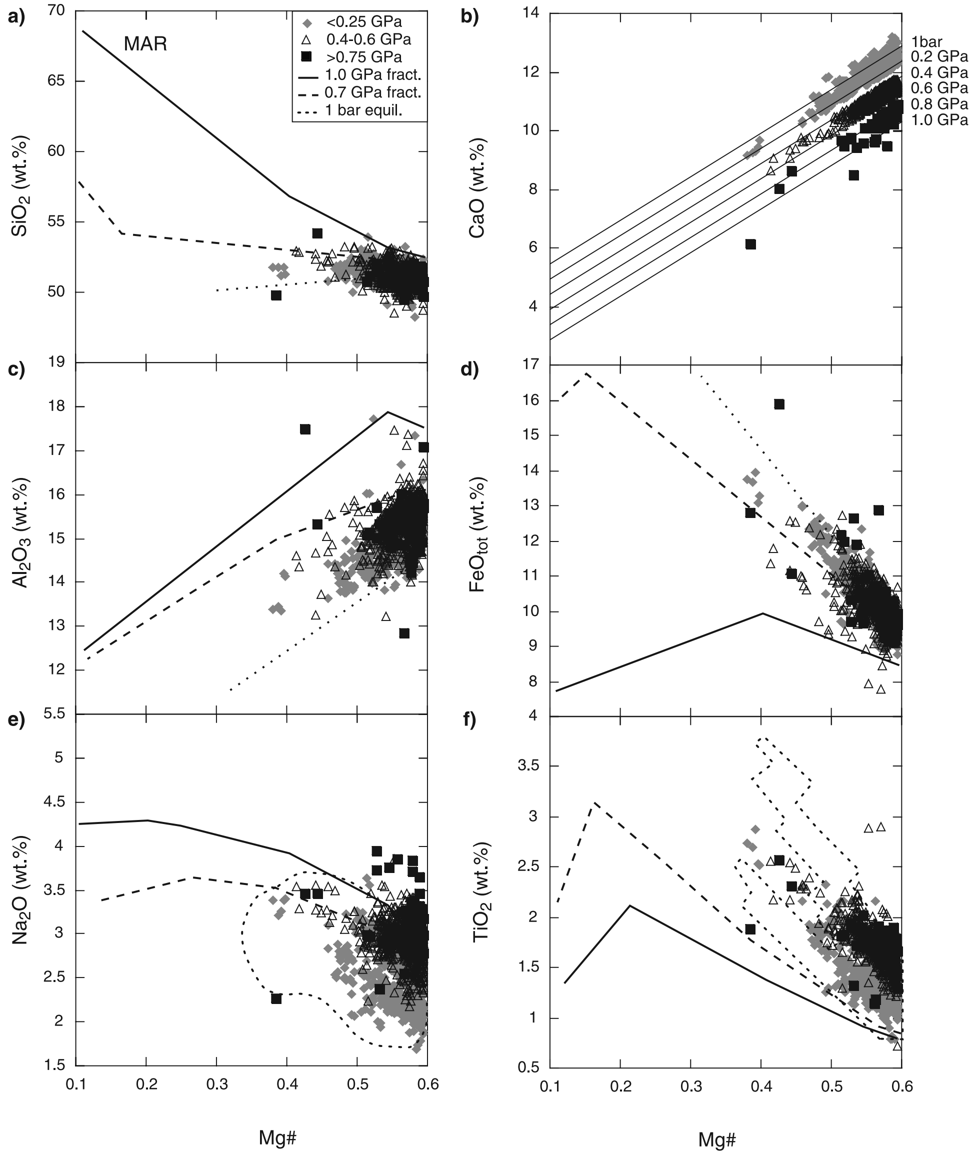

Figure 10. Variation diagrams of (a) SiO_2, (b) CaO, (c) Al_2O_3, (d) FeO_{tot}, (e) Na_2O, and (f) TiO_2 in wt % plotted against Mg # from glasses of the Mid-Atlantic Ridge (MAR). Glass compositions are grouped into three classes of calculated crystallization pressures. Pressure <0.25 GPa, gray diamonds; pressure 0.4–0.6 GPa, open triangles; pressure >0.75 GPa, black squares. Lines mark the liquid lines of descent of fractional crystallization experiments at 0.7 GPa (dashed line) and at 1.0 GPa (straight line). Small dashes indicate the average of experimental glasses at 1 bar.

unlike EPR glasses, they do not reach highly differentiated compositions (Mg # < 0.4). Interestingly, none of the high-pressure MAR glasses follow the fractional crystallization trends at 1.0 GPa in terms of SiO_2, Al_2O_3, and FeO_{tot}, but plot within the region of equilibrium crystallization experiments at ~0.8 GPa. Compared to the high-pressure glasses from the EPR, they are characterized by lower SiO_2 and higher FeO_{tot} contents at a given Mg #, which reflect a higher mean pressure of mantle melting. Na_2O (Figure 10e) and TiO_2 (Figure 10f) at a given Mg # are generally higher with increasing pressure of crystallization. As at the EPR, incompatible element variations of MAR glasses crystallized near transform faults reflect lower degrees of partial melting, possibly due to the transform fault effect (Kane region: [*Langmuir and Bender*, 1984; *Ghose et al.*, 1996]).

4.3. Southwest Indian Ridge (5°W–75°E)

[30] Compared with the EPR or the MAR only a small data set exists along the SWIR between 5°W and 75°E. The average calculated pressure of 229 SWIR glasses is 0.55 ± 0.29 GPa (Figure 11a). Estimated pressures for all SWIR glasses plotted as a histogram (white boxes) show a bimodal distribution of crystallization pressures (Figure 6c), but the data set is strongly determined by two large areas, as shown in Figure 11. The samples from the Atlantis II Fracture Zone represent about 41% of the whole data set. Thirty-seven percent of the data are from locations along the SWIR with

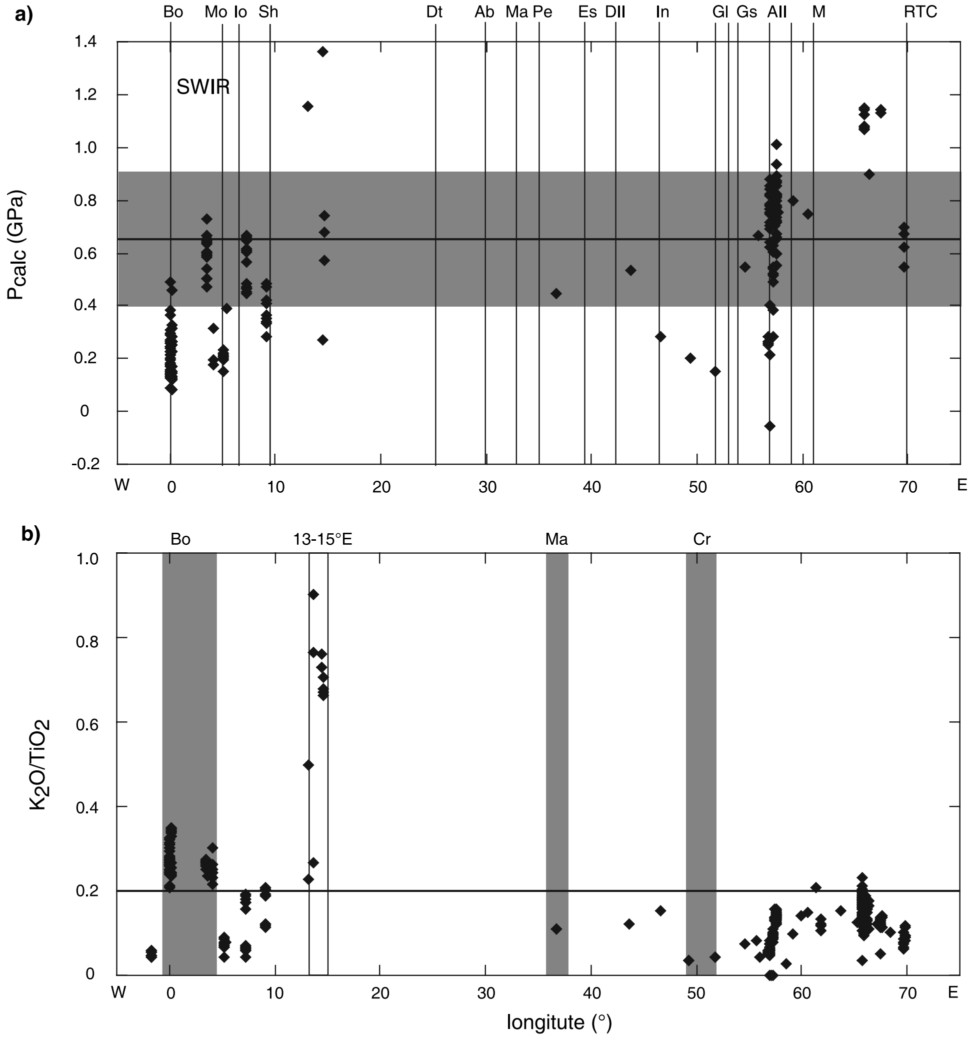

Figure 11. (a) Calculated pressures for glasses of basalts form the Southwest Indian Ridge (SWIR) between 5°W and 75°E plotted against longitude. For pressure calculations with the CaO–Mg # barometer, glass analyses have been normalized to 100% and glasses with Mg # < 0.6 were used. The horizontal line represents the average pressure of 0.66 GPa of 145 glasses from ridge segments possibly not affected by hot spots. The gray shaded area defines their standard deviation of ±0.26 GPa. Vertical lines mark the positions of fracture zones (FZ): Bo, Bouvet; Mo, Moshesh; Io, Islas Orcadas; Sh, Shaka; Dt, Du Toit; Ab, Andrew Bain; Ma, Marion; Pe, Prince Edward; Es, Eric Simpson; DII, Discovery II; In, Indomed; Gl, Gallieni; Gs, Gauss; AII, Atlantis II; M, Mellville; RTC, Rodriguez Indian Ocean triple junction. (b) K_2O/TiO_2 ratios of glasses plotted against latitude. Horizontal black line marks a K_2O/TiO_2 ratio of 0.2. Gray vertical boxes indicate regions of possibly hot spot influenced ridge sections: Bou, Bouvet; Ma, Marion; Cr, Crozet hot spot. White box, additional ridge segment with enriched K_2O/TiO_2 ratios (13°E–15°E anomaly).

elevated K_2O/TiO_2 ratios (Figure 11b). Between 0° and 4°E the Bouvet hot spot influences the SWIR [*le Roex et al.*, 1983, *Goslin et al.*, 1999; *Georgen et al.*, 2001], and between 13°E and15°E an anomaly with unusually high K_2O/TiO_2 ratios and relative enrichment of highly incompatible elements [*le Roex et al.*, 1992; *Janney et al.*, 2005] shows little evidence for low-pressure fractionation. Along the SWIR between 15°E and 55°E, the small number of glass analyses does not permit straightforward conclusions, but it is well known that the Marion and Crozet hot spots may influence ridge chemistry [*le Roex et al.*, 1989; *Mahoney et al.*, 1992; *Georgen et al.*, 2001; *Janney et al.*, 2005; *Meyzen et al.*, 2005]. Filtering potential hot spot influenced glass analyses from the data set eliminates most of the low-pressure data (Figure 6c). The average crystallization pressure of 145 'normal' SWIR glasses result in 0.66 ± 0.26 GPa. Only 10.4% of the 'normal' SWIR glasses have been crystallized below 0.25 GPa; 24.1% are within 0.3 to 0.55 GPa; 53.8% of the glasses show pressures between 0.6 and 0.9 GPa and for 11.7% of the glasses, pressures exceeding 0.9 GPa have been obtained.

[31] Selected oxides of SWIR glasses plotted against Mg # < 0.6 are shown in Figure 12. As discussed above, the glass analyses for the SWIR were grouped in the same three classes of calculated crystallization pressures (P < 0.25 GPa, P = 0.4–0.6 GPa, P > 0.75 GPa) shown by Figure 12b.

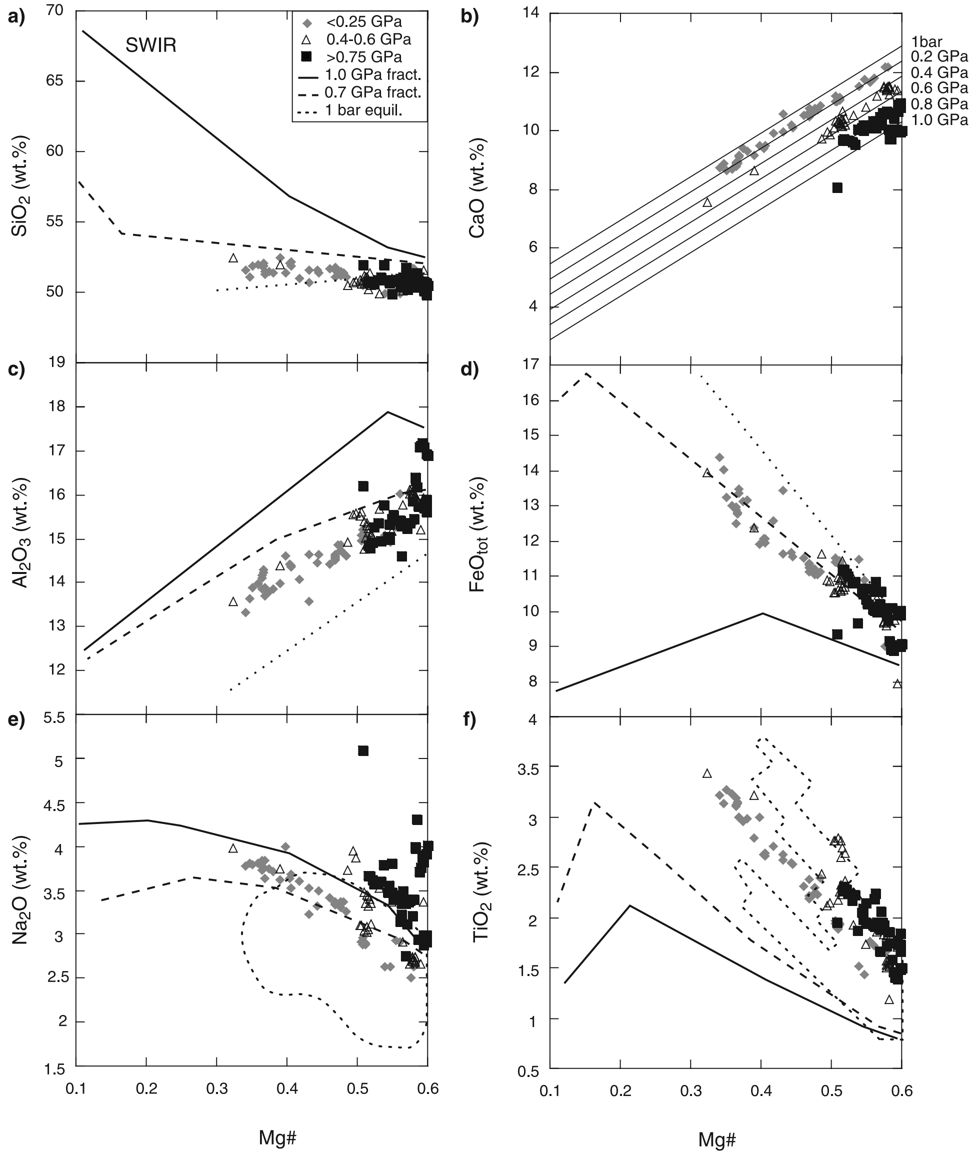

Figure 12. Variation diagrams of (a) SiO_2, (b) CaO, (c) Al_2O_3, (d) FeO_{tot}, (e) Na_2O, and (f) TiO_2 in wt % plotted against Mg # from glasses of the Southwest Indian Ridge. Glass compositions are grouped into three classes of calculated crystallization pressures. Pressure<0.25 GPa, gray diamonds; pressure 0.4–0.6 GPa, open triangles; pressure >0.75 GPa, black squares. Lines mark the liquid lines of descent of fractional crystallization experiments at 0.7 GPa (dashed line) and at 1.0 GPa (straight line). Small dashes indicate the average of experimental glasses at 1 bar.

Similar to the MAR glasses, the differentiation trends of the SWIR glasses do not reach highly differentiated compositions. SWIR glasses that crystallized above 0.75 GPa include samples that have Mg # as low as 0.5. Regardless of the crystallization pressure of SWIR glasses, SiO_2 (Figure 12a) exhibits a moderate increase from 49 to 52 wt %. The Al_2O_3 contents of the low-pressure SWIR glasses plot at the higher end of EPR and MAR fractionation trends (compare Figure 12c with Figures 8c and 10c). This might reflect lower degrees of partial melting along the SWIR. FeO_{tot} of the SWIR glasses evolves along a flatter slope than glasses of the EPR and MAR (Figure 12d). Na_2O of the low-pressure glasses (Figure 12e) plots at the higher end of the experimental liquid lines of descent at 1 bar. The intermediate- and high-pressure glasses are spread from similar Na_2O values up to over 4 wt % at similar Mg #, indicating low degrees of partial melting. TiO_2 of the SWIR glasses evolves like TiO_2 in the EPR glasses but at the higher end of the MAR differentiation trend (Figure 12f).

5. Discussion

5.1. Crystallization Pressures Along Mid-ocean Ridges

[32] Crystallization pressures of MORB suites have been estimated by various methods as discussed above. *Grove et al.* [1992] estimated crystallization pressures of basalts from the Cayman spreading center, the EPR (10°–11°N) and near the Kane Fracture Zone region. *Yang et al.* [1996] applied their model to EPR glasses. *Michael and Cornell* [1998] compared crystallization pressures estimated by inversion of

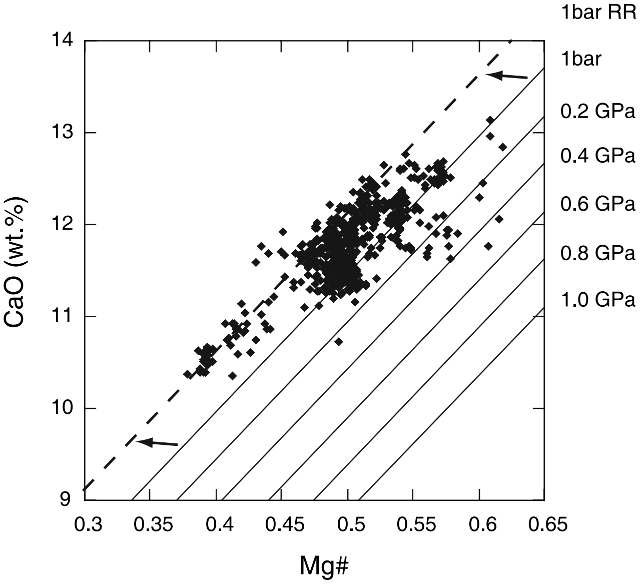

Figure 13. Variation diagram of CaO (wt %) plotted against Mg # of glass compositions from the Reykjanes Ridge. Dashed line, shifted 1 bar isobar to higher CaO contents.

the model of *Yang et al.* [1996] with numerical models of *Danyushevsky et al.* [1996] and *Weaver and Langmuir* [1990], and applied them to an extended MORB database. *Herzberg* [2004] calculated crystallization pressures with a new parameterization (discussed above) applied to a large MORB database. All these methods, including our new CaO/Mg # barometer, utilize the pressure-dependent liquidus boundaries of clinopyroxene, olivine and plagioclase in tholeiitic systems. All barometers indicate that glasses from most MORB suites must have crystallized cpx at some stage in their evolution. As cpx is not very abundant in mid-ocean ridge lavas, it has been dissolved or removed by crystal settling during the ascent of the MORB lavas. This "pyroxene paradox" has been discussed in several studies [*Thompson et al.*, 1980; *Fisk et al.*, 1980; *Fujii and Bougault*, 1983; *Grove et al.*, 1992; *Elthon et al.*, 1995] and is related to the expansion of the ol and plg stability fields at low pressure with respect to cpx, as shown by several experimental studies [*Green and Ringwood*, 1967; *Bender et al.*, 1978; *Baker and Eggler*, 1987; *Gust and Perfit*, 1987; *Grove et al.*, 1992]. Application of the various barometers to a wide variety of "normal" MORB indicates a clear correlation between crystallization pressure and spreading rate. The fast spreading EPR is dominated by basalts equilibrated at low pressure and highly differentiated basalts. Such highly differentiated basalts are apparently rare in slower spreading areas (Figures 10 and 12).

[33] Similarly, glasses from the Reykjanes Ridge are interpreted as products of low-pressure crystallization [*Herzberg*, 2004]. Along the liquid line of descent of the Reykjanes Ridge, the CaO/Mg # ratio is similar to the experimental data but is shifted toward lower Mg # at a given CaO content (Figure 13). Consequently, the application of the CaO/Mg # barometer results in negative calculated crystallization pressures. The shift of the cpx-in phase boundary toward lower Mg # compared with normal MORB (about 0.05) is readily explained by a mantle composition that is unusually Fe-rich. *Korenaga and Kelemen* [2000] calculated Mg # in equilibrium with primary liquids from the North Atlantic igneous province and concluded that the mantle underneath Iceland is unusually Fe-rich. An alternative possibility is that Reykjanes Ridge glasses crystallized from H_2O-rich magmas, with a prolonged interval of olivine crystallization and corresponding enrichment of CaO.

[34] Elevated crystallization pressures are obtained for medium and slow spreading ridges like the Southeast Indian Ridge, the MAR, the Mohns and Knipovitch Ridge, the SWIR and the Cayman Spreading Center.

[35] *Dimitriev* [1998], *LeRoux et al.* [2002] and *Herzberg* [2004] plotted estimated crystallization pressures against latitude for different MORB suites. All of these studies conclude that elevated pressures may preferentially be observed in the regions of ridge terminations like fracture zones, overlapping spreading centers and deviations from axial linearity. Segments of slow spreading ridges associated with hot spots (e.g., Azores Plateau, and Bouvet) display both low-pressure crystallization as well as crystallization pressures up to 1.0 GPa around fracture zones.

5.2. Evidence for Crystallization of MORB Within the Mantle

[36] Most glasses from fast spreading ridges and hot spot-influenced slow spreading ridges result in calculated crystallization pressures lower than ~0.25 GPa. However, slow and ultraslow spreading ridges show elevated crystallization pressures for a substantial fraction of MORB. As the cpx phase volume is expanded relative to plagioclase at high pressure, the chemistry of MORB from slow spreading ridges requires extensive crystallization of cpx-bearing cumulates within the upper mantle. Evidence for melt/rock reaction and partial crystallization of basaltic magma is well known from mid-ocean ridges [*Dick*, 1989; *Elthon*, 1992; *Cannat and Casey*, 1995; *Cannat et al.*, 1997; *Seyler and Bonatti*, 1997]. There is abundant evidence for crystallization of MORB type magmas in ophiolites [e.g., *Rampone et al.*, 1997; *Müntener and Piccardo*, 2003; *Müntener et al.*, 2004]. On the basis of field observations and geochemical data *Müntener and Piccardo* [2003] presented a conceptual model for melt migration by pervasive porous melt flow evolving to focused porous flow and finally to diking. The consequences are that substantial amounts of MORB might be trapped in the upper mantle. These observations are supported by recently drilled mantle sections along the MAR 14°–16°N, which recovered impregnated mantle peridotite and gabbroic intrusions up to a few meters across [*Kelemen et al.*, 2004]. The average of calculated crystallization pressures of 0.53 ± 0.1 GPa of glasses around the 15°20' Fracture Zone is in good agreement with gabbroic intrusions within the upper mantle.

5.3. Crystallization and Mantle Partial Melting Below Mid-ocean Ridges

[37] Compared to experimental data, major element variations of three typical mid-ocean ridge systems with spreading rates ranging from ultraslow to fast demonstrate crystallization at various pressures as well as derivation from primary liquids that represent variable melt fractions

derived from partially molten peridotite. The degree of partial melting estimated from Na_2O variations decreases with increasing crystallization pressures. Averaged Na_8 of glasses from the entire database of each of the three ridges roughly correlate with crystallization pressure calculated with the CaO/Mg # barometer and with the methods discussed above [*Michael and Cornell*, 1998], but Na_8 values overlap for individual groups of crystallization pressure. *Klein and Langmuir* [1987] showed a rough correlation of Na_8 as an indicator of the extent of partial melting of peridotite with crustal thickness and axial depth. In general, axial depths and crustal thickness increase approaching transform faults [*White et al.*, 1984, 2001; *Bown and White*, 1994; *Muller et al.*, 1999, 2000]. *Bown and White*'s [1994] modeling and *Reid and Jackson*'s [1981] seismic studies suggest that the effect of a thicker lithosphere on the upper limit of melting is only seen at spreading rates <2 cm/yr (full rate). At spreading rates >2 cm/yr, the crustal thickness is approximately constant, and therefore the lithosphere thickness is not strongly variable. *Michael and Cornell* [1998] pointed out that different crystallization pressures are related to the magma flux and advected heat below the spreading center and are dependent on spreading rate and extent of melting.

[38] Crystallization of basaltic liquids initiates when the temperature of the ambient peridotite drops below the basalt liquidus. The highest calculated crystallization pressures may provide an upper bound on the pressure at the top of the mantle-melting region below slow spreading ridges, which has been estimated to range between 1.0 GPa and 1.5 GPa for the southern MAR [*LeRoux et al.*, 2002]. Low degrees of melting at high pressure was indicated by Rare Earth Element modeling of samples from ultraslow spreading ridges (e.g., SWIR, Gakkel Ridge, Knipovitch Ridge, Mohns Ridge, Cayman Trough) [*White et al.*, 2001]. Low degrees of partial melting in the presence of small amounts of H_2O was inferred for the origin of the SWIR lavas [*Robinson et al.*, 2001]. Both studies included conductive cooling in their models. The lithosphere along slow spreading ridges is thicker than at fast spreading ridges so that conductive cooling generally reaches deeper into the mantle [*Reid and Jackson*, 1981; *Shen and Forsyth*, 1995; *Bown and White*, 1994; *White et al.*, 2001]. Variable depths of crystallization along mid-ocean ridges thus require variations in topography of the melting region and in lithospheric thickness. *Langmuir et al.* [1984] termed such variations "transform fault effects," which have been proposed by *Bender et al.* [1984] and *Langmuir et al.* [1986] for the EPR, by *Ghose et al.* [1996] and *Reynolds and Langmuir* [1997] for the Kane Fracture Zone and by *LeRoux et al.* [2002] for the southern MAR (55°–40°S).

[39] For fast spreading ridges, is not possible to estimate the top of the melting region by the method of crystallization pressures, because the potential high-pressure signature of basaltic glasses was most probably erased by reequilibration in shallow crustal magma chambers [*Herzberg*, 2004]. Along fracture zones where high-pressure crystallization signatures are still preserved in the glasses, the consistent SiO_2 enrichment and low FeO contents may be a result of shallower melting compared to slow spreading ridges. Na_2O variations and Na_8 of high-pressure glasses reflect lower degrees of partial melting at ridge terminations, which is consistent with the observations of *Le Mée et al.* [2004]. They reported along-axis variations of Cr# [molar Cr/(Cr + Al)] in spinel and variations in Yb/Er of harzburgites from the fossil fast spreading mid-ocean ridge of the Oman ophiolite. Long-wavelength variations are consistent with the paleoridge segmentation, which mark the ends of main magmatic cells. The decrease in the degree of partial melting toward paleofracture zones roughly correlates with decreasing lower crustal thickness, interpreted as zones with lower magma production.

6. Conclusions

[40] Estimation of crystallization pressures of basaltic magmas based on the compositions of quenched glasses has been done in the past. Nevertheless, plotting CaO (wt %) against Mg # [= Mg/(Mg + Fe), all Fe as Fe^{2+}] of basaltic glasses with Mg # < 0.6 and using equation (2) provides an independent method to estimate crystallization pressures of MORB of variable compositions in equilibrium with cpx. The pressure estimates are comparable with those calculated with the inverted X_{Ca} equation of *Yang et al.* [1996]. The use of 1.0 GPa fractional crystallization experiments covering a wide range of Mg # in our calibration favors our barometer for differentiated compositions, especially at high pressures.

[41] Basalts at segments of mid-ocean ridges assumed to have underlying magma chambers record preferentially crustal crystallization pressures (<0.25 GPa). The chemical signatures of mid-ocean ridge basalts at ridge segments without crustal magma chambers and at ridge terminations show evidence for high-pressure fractionation, up to 1.0 GPa. At normal ridge sections (unaffected by hot spots), the crystallization of gabbroic cumulates takes place at shallow crustal levels, reaching minimum depths corresponding to pressures of ~0.3 GPa for fast spreading ridges like the EPR. For slow spreading ridges the principal crystallization starts within the mantle at pressures between 0.3 and 0.7 GPa (MAR) and between 0.4 and 0.8 GPa (SWIR).

[42] A comparison between experimental glass composition and glasses from mid-ocean ridges as a function of crystallization pressure shows that the liquid lines of descent defined by natural MORB can be simulated reasonably well by equilibrium and fractional crystallization experiments at similar pressures.

[43] Incompatible-element characteristics of basalts that crystallized at high pressures indicate lower degrees of partial melting of the underlying mantle, favoring models of melting regions with topography, which require enhanced conductive cooling below 'normal' slow spreading ridges and at ridge terminations for both fast and slow spreading ridges.

[44] **Acknowledgments.** This research was supported by the Swiss National Science Foundation (grant 2000-61894.00/1). We thank Tim Grove and Alan Thompson for comments, Deborah Eason and Peter Michael for constructive reviews, and John Mahoney for many editorial comments that substantially improved the paper.

References

Ariskin, A. A. (1999), Phase equilibria modeling in igneous petrology: Use of COMAGMAT model for simulating fractionation of ferro-basaltic magmas and the genesis of high-alumina basalt, *J. Volcanol. Geotherm. Res.*, *90*, 115–162.

Ariskin, A. A., M. Y. Frenkel, G. S. Barmina, and R. L. Nielsen (1993), COMAGMAT: A Fortran program to model magma differentiation processes, *Comput. Geosci.*, *19*, 1155–1170.

Baker, D. R., and D. H. Eggler (1987), Compositions of anhydrous and hydrous melts coexisting with plagioclase, augite, and olivine or low-Ca pyroxene from 1 atm to 8 kbar: Application to Aleutian volcanic center of Atka, *Am. Mineral.*, *72*, 12–28.

Baker, M. B., M. M. Hirschmann, M. S. Ghiorso, and E. M. Stolper (1995), Compositions of near-solidus peridotite melts from experiments and thermodynamic calculations, *Nature*, *375*, 308–311.

Bartels, K. S., R. J. Kinzler, and T. L. Grove (1991), High pressure phase relations of primitive high-alumina basalts from Medicine Lake volcano, northern California, *Contrib. Mineral. Petrol.*, *108*, 253–270.

Bender, J. F., F. N. Hodges, and A. E. Bence (1978), Petrogenesis of basalts from the project FAMOUS area: Experimental study from 0 to 15 kbar, *Earth Planet. Sci. Lett.*, *41*, 277–302.

Bender, J. F., C. H. Langmuir, and G. N. Hanson (1984), Petrogenesis of basalt glasses from the Tamayo Region, East Pacific Rise, *J. Petrol.*, *25*, 213–254.

Berndt, J., J. Koepke, and F. Holtz (2005), An experimental investigation of the influence of water and oxygen fugacity on differentiation of MORB at 200 MPa, *J. Petrol.*, *46*, 135–167.

Bowen, N. L. (1928), *The Evolution of Igneous Rocks*, Princeton Univ. Press, Princeton, N. J.

Bown, J. W., and R. S. White (1994), Variation with spreading rate of oceanic crustal thickness and geochemistry, *Earth Planet. Sci. Lett.*, *121*, 435–449.

Cannat, M., and J. F. Casey (1995), An ultramafic lift at the Mid-Atlantic Ridge: Successive stages of magmatism in serpentinized peridotites from the 15°N region, in *Mantle and Lower Crust Exposed in Oceanic Ridges and in Ophiolites*, edited by R. L. M. Vissers and A. Nicolas, pp. 5–34, Springer, New York.

Cannat, M., F. Chatin, H. Witechurch, and G. Ceuleneer (1997), Gabbroic rocks trapped in the upper mantle at the Mid-Atlantic Ridge, *Proc. Ocean Drill. Program Sci. Results*, *153*, 243–264.

Danyushevsky, L. V., A. V. Sobolev, and L. V. Dimitriev (1996), Estimation of the pressure of crystallization and H_2O content of MORB and BABB glasses: Calibration of an empirical technique, *Mineral. Petrol.*, *57*, 185–204.

Dick, H. J. B. (1989), Abyssal peridotites, very slow spreading ridges and ocean ridge magmatism, in *Magmatism in the Ocean Basins*, edited by A. D. Saunders and M. J. Norry, *Spec. Publ. Geol. Soc. London*, *42*, 71–105.

Dimitriev, L. (1998), Chemical variations of mid ocean ridge basalts as a function of the geodynamic setting of their formation, *Petrology*, *6*, 314–334.

Elthon, D. (1979), High magnesia liquids as the parental magma for ocean floor basalts, *Nature*, *278*, 514–518.

Elthon, D. (1992), Chemical trends in abyssal peridotites: Refertilization of depleted suboceanic mantle, *J. Geophys. Res.*, *97*, 9015–9025.

Elthon, D., and C. M. Scarfe (1984), High-pressure phase equilibria of a high-magnesia basalt and the genesis of primary oceanic basalts, *Am. Mineral.*, *69*, 1–15.

Elthon, D., D. K. Ross, and J. K. Meen (1995), Compositional variations of basaltic glasses from the Mid-Cayman Rise spreading center, *J. Geophys. Res.*, *100*, 12,497–12,512.

Falloon, T. J., and D. H. Green (1987), Anhydrous partial melting of MORB pyrolite and other peridotite compositions at 10 kbar: Implications for the origin of primitive MORB glasses, *Mineral. Petrol.*, *37*, 181–219.

Falloon, T. J., and D. H. Green (1988), Anhydrous partial melting of peridotite from 8 to 35 kb and the petrogenesis of MORM, *J. Petrol.*, *29*, 379–414.

Fisk, M. R., J. G. Schilling, and H. Sigurdsson (1980), An experimental investigation of Iceland and Reykjanes Ridge tholeiites: I. Phase relations, *Contrib. Mineral. Petrol.*, *74*, 361–374.

Fram, M. S., and J. Longhi (1992), Phase equilibria of dikes associated with Proterozoic anorthosite complexes, *Am. Mineral.*, *77*, 605–616.

Fujii, T., and H. Bougault (1983), Melting relations of a magnesian abyssal tholeiite and the origin of MORBs, *Earth Planet. Sci. Lett.*, *63*, 283–295.

Georgen, J., J. Lin, and H. J. B. Dick (2001), Evidence from gravity anomalies for interactions Marion and Bouvet hotspots with the Southwest Ridge: Effects of transform offsets, *Earth Planet. Sci. Lett.*, *187*, 283–300.

Ghiorso, M. S., and R. O. Sack (1995), Chemical mass transfer in magmatic processes IV: A revised and internally consistent thermodynamic model for the interpretation and extrapolation of liquid-solid equilibria in magmatic systems at elevated temperatures and pressures, *Contrib. Mineral. Petrol.*, *119*, 197–212.

Ghiorso, M. S., M. M. Hirschmann, P. W. Reiners, and V. C. Kress III (2002), The pMELTS: A revision of MELTS for improved calculation of phase relations and major element partitioning related to partial melting of the mantle to 3 GPa, *Geochem. Geophys. Geosyst.*, *3*(5), 1030, doi:10.1029/2001GC000217.

Ghose, I., M. Cannat, and M. Seyler (1996), Transform fault effect on mantle melting in the MARK area (Mid-Atlantic Ridge south of the Kane transform), *Geology*, *24*, 1139–1142.

Goslin, J., J.-L. Thirot, O. Noel, and J. Francheteau (1999), Slow ridge/hotspot interactions from global gravity, seismic tomography and $^{87}Sr/^{86}Sr$ isotope data, *Geophys. J. Int.*, *135*, 700–710.

Green, D. H., and A. E. Ringwood (1967), The genesis of basaltic magmas, *Contrib. Mineral. Petrol.*, *15*, 103–190.

Grove, T. L., and W. B. Bryan (1983), Fractionation of pyroxene-phyric MORB at low pressure: An experimental study, *Contrib. Mineral. Petrol.*, *84*, 293–309.

Grove, T. L., R. J. Kinzler, and W. B. Bryan (1990), Natural and experimental phase relations of lavas from Serocki volcano, *Proc. Ocean Drill. Program Sci. Results*, *106*, 9–17.

Grove, T. L., R. J. Kinzler, and W. B. Bryan (1992), Fractionation of mid-ocean ridge basalt (MORB), in *Mantle Flow and Melt Generation at Mid-Ocean Ridges*, *Geophys. Monogr. Ser.*, vol. 71, edited by J. Phipps Morgan, D. K. Blackman, and J. M. Sinton, pp. 281–310, AGU, Washington, D. C.

Gust, D. A., and M. R. Perfit (1987), Phase relations of a high-Mg basalt from the Aleutian Island Arc: Implications for primary island arc basalts and high Al basalts, *Contrib. Mineral. Petrol.*, *97*, 7–18.

Herzberg, C. (2004), Partial crystallization of mid-ocean ridge basalts in the crust and mantle, *J. Petrol.*, *45*, 2389–2405.

Hirschmann, M. M., M. S. Ghiorso, L. E. Wasylenki, P. D. Asimov, and E. M. Stolper (1998), Calculation of peridotite partial melting from thermodynamic models of minerals and melts. I. Review of methods and comparison with experiments, *J. Petrol.*, *39*, 1091–1115.

Hirschmann, M. M., M. S. Ghiorso, L. E. Wasylenki, P. D. Asimov, and E. M. Stolper (1999), Calculation of peridotite partial melting from thermodynamic models of minerals and melts. II. Isobaric variations in melts near the solidus and owing to variable source composition, *J. Petrol.*, *40*, 297–313.

Hirth, G., and D. L. Kohlstedt (1996), Water in the oceanic upper mantle: Implications for rheology, melt extraction and the evolution of the lithosphere, *Earth Planet. Sci. Lett.*, *144*, 93–108.

Janney, P. E., A. P. Le Roex, and R. W. Carlson (2005), Hafnium isotope and trace element constraints on the nature of mantle heterogeneity beneath the central Southwest Indian Ridge (13°E to 47°E), *J. Petrol.*, *46*, 2427–2464.

Kelemen, P., G. Hirth, N. Shimizu, M. Spiegelman, and H. J. B. Dick (1997), A review of melt migration processes in the asthenospheric mantle beneath oceanic spreading centers, *Philos. Trans. R. Soc. London, Ser. A*, *355*, 283–318.

Kelemen, P. B., E. Kikawa, and D. J. Miller (2004), *Drilling Mantle Peridotite Along the Mid-Atlantic Ridge From 14° to 16°N, Proceedings of the Ocean Drilling Program*, *Initial Report* [CD-ROM], vol. 209, Ocean Drill Program, College Station, Tex. (Available at http://www-odp.tamu.edu/publications/209_IR/209ir.htm)

Kinzler, R. J., and T. L. Grove (1992), Primary magmas of mid-ocean ridge basalts: 1. Experiments and methods, *J. Geophys. Res.*, *97*, 6885–6906.

Klein, E. M., and C. H. Langmuir (1987), Global correlation of ocean ridge basalt chemistry with axial depth and crustal thickness, *J. Geophys. Res.*, *92*, 8089–8115.

Korenaga, J., and P. Kelemen (2000), Major element heterogeneity in the mantle source of the North Atlantic igneous province, *Earth Planet. Sci. Lett.*, *184*, 251–268.

Kushiro, I. (1969), The system forsterite-diopside-silica with and without water at high pressures, *Am. J. Sci.*, *267*, 269–294.

Kushiro, I. (2001), Partial melting experiments on peridotite and origin of mid-ocean ridge basalt, *Annu. Rev. Earth Planet. Sci.*, *29*, 71–107.

Langmuir, C. H., and J. F. Bender (1984), The geochemistry of oceanic basalts in the vicinity of transform faults: Observation and implications, *Earth Planet. Sci. Lett.*, *69*, 107–127.

Langmuir, C. H., J. F. Bender, and R. Batiza (1986), Petrological and tectonic segmentation of the East Pacific Rise, 5°30′–14°30′N, *Nature*, *322*, 422–429.

Langmuir, C. H., E. M. Klein, and T. Plank (1992), Petrological systematics of mid-ocean ridge basalts: Constraints on melt generation beneath ocean ridges, in *Mantle Flow and Melt Generation at Mid-Ocean Ridges*, *Geophys. Monogr. Ser.*, vol. 71, edited by J. Phipps Morgan, D. K. Blackman, and J. M. Sinton, pp. 183–280, AGU, Washington, D. C.

Le Mée, L., J. Girardeau, and C. Monnier (2004), Mantle segmentation along the Oman ophiolite fossil mid-ocean ridge, *Nature*, *432*, 167–172.

le Roex, A. P., H. J. B. Dick, A. J. Erlank, A. M. Reid, F. A. Frey, and S. R. Hart (1983), Geochemistry, mineralogy and petrogenesis of lavas erupted along the Southwest Indian Ridge between the Bouvet triple junction and 11 degrees east, *J. Petrol.*, *24*, 267–318.

le Roex, A. P., H. J. B. Dick, and R. L. Fisher (1989), Petrology and geochemistry of MORB from 25°E to 46°E along the Southwest Indian Ridge: Evidence for contrasting styles of mantle enrichment, *J. Petrol.*, *30*, 947–986.

le Roex, A. P., H. J. B. Dick, and R. T. Watkins (1992), Petrogenesis of anomalous K-enriched MORB from the Southwest Indian Ridge: 11°53′E to 14°38′E, *Contrib. Mineral. Petrol.*, *110*, 253–268.

LeRoux, P. J., A. P. le Roex, and J. G. Schilling (2002), Crystallization processes beneath the southern Mid-Atlantic Ridge (40°–55°S), evidence for high-pressure initiation of crystallization, *Contrib. Mineral. Petrol.*, *143*, 582–602.

Macdonald, K. C., P. J. Fox, L. J. Perram, M. F. Eisen, R. M. Haymon, S. P. Miller, S. M. Carbotte, M. H. Cormier, and A. N. Shor (1988), A new view of the mid-ocean ridge from the behavior of ridge-axis discontinuities, *Nature*, *335*, 217–225.

Mahoney, J., A. P. le Roex, Z. Peng, R. L. Fisher, and J. H. Natland (1992), Southwestern limits of Indian ocean ridge mantle and origin of low ^{206}Pb/^{204}Pb mid-ocean ridge basalt: Isotope systematics of the central Southwest Indian Ridge (17°–50°E), *J. Geophys. Res.*, *97*, 19,771–19,790.

Meyzen, C., J. N. Ludden, E. Humler, B. Luais, M. J. Toplis, C. Mevel, and M. Storey (2005), New insights into the origin and distribution of the DUPAL isotope anomaly in the Indian Ocean mantle from MORB of the Southwest Indian Ridge, *Geochem. Geophys. Geosyst.*, *6*, Q11K11, doi:10.1029/2005GC000979.

Michael, P. J., and W. C. Cornell (1998), Influence of spreading rate and magma supply on crystallization and assimilation beneath mid-ocean ridges: Evidence from chlorine and major element chemistry of mid-ocean ridge basalts, *J. Geophys. Res.*, *103*, 18,325–18,356.

Muller, M. R., T. A. Minshull, and R. S. White (1999), Segmentation and melt supply at the Southwest Indian Ridge, *Geology*, *27*, 867–870.

Muller, M. R., T. A. Minshull, and R. S. White (2000), Crustal structure of the Southwest Indian Ridge at the Atlantis II Fracture Zone, *J. Geophys. Res.*, *105*, 25,809–25,828.

Müntener, O., and G. B. Piccardo (2003), Melt migration in ophiolitic peridotites: The message from Alpine-Apennine peridotites and implications for embryonic ocean basins, in *Ophiolites in Earth History*, edited by Y. Dilek and P. T. Robinson, *Spec. Publ. Geol. Soc. London*, *217*, 69–89.

Müntener, O., T. Pettke, L. Desmurs, M. Meier, and U. Schaltegger (2004), Refertilization of mantle peridotite in embryonic ocean basins: Trace element and Nd-isotopic evidence and implications for crust-mantle relationships, *Earth Planet. Sci. Lett.*, *221*, 93–108.

Navin, A. D., C. Peirce, and M. C. Sinha (1998), The RAMESSES experiment; II, Evidence for accumulated melt beneath a slow spreading ridge from wide angle refraction and multichannel reflection seismic profiles, *Geophys. J. Int.*, *135*, 746–772.

Niu, Y., and R. Hékinian (1997), Basaltic liquids and harzburgitic residues in the Garret Transform: A case study at fast spreading ridges, *Earth Planet. Sci. Lett.*, *146*, 243–258.

Pallister, J. S., and C. A. Hopson (1981), Samail Ophiolite plutonic suite: Field relations, phase variation, cryptic variation and layering, and a model of a spreading ridge magma chamber, *J. Geophys. Res.*, *86*, 2593–2644.

Perfit, M. R., et al. (1996), Recent volcanism in the Siqueiros Transform fault: Picritic basalts and implication for MORB magma genesis, *Earth Planet. Sci. Lett.*, *141*, 91–108.

Pockalny, R. A., P. J. Fox, D. J. Fornari, K. C. Macdonald, and M. R. Perfit (1997), Tectonic reconstruction of the Clipperton and Siqueiros fracture zones: Evidence and consequences of plate motion change for the last 3 myr, *J. Geophys. Res.*, *102*, 3167–3181.

Rampone, E., G. B. Piccardo, R. Vannucci, and P. Bottazzi (1997), Chemistry and origin of trapped melts in ophiolitic peridotites, *Geochim. Cosmochim. Acta*, *61*, 4557–4569.

Reid, I., and H. R. Jackson (1981), Oceanic spreading rate and crustal thickness, *Mar. Geophys. Res.*, *5*, 165–172.

Reynolds, J. R., and C. Langmuir (1997), Petrological systematics of the Mid-Atlantic Ridge south of Kane: Implications for ocean crust formation, *J. Geophys. Res.*, *102*, 14,915–14,946.

Reynolds, J. R., C. Langmuir, J. F. Bender, K. A. Kastens, and W. B. F. Ryan (1992), Spatial and temporal variability in the geochemistry of basalts from the East Pacific Rise, *Nature*, *359*, 493–499.

Robinson, C. J., M. J. Bickle, T. A. Minshull, R. S. White, and A. R. L. Nichols (2001), Low degree melting under the Southwest Indian Ridge: The roles of mantle temperature, conductive cooling and wet melting, *Earth Planet. Sci. Lett.*, *188*, 383–398.

Sano, T., T. Fujii, S. S. Deshmukh, T. Fukuoka, and S. Aramaki (2001), Differentiation process of Deccan Trap basalts: Contribution from geochemistry and experimental petrology, *J. Petrol.*, *42*, 2175–2195.

Schilling, J. G. (1975), Azores mantle blob: Rare-Earth evidence, *Earth Planet. Sci. Lett.*, *25*, 103–115.

Seyler, M., and E. Bonatti (1997), Regional-scale melt-rock interaction in lherzolitic mantle in the Romanche fracture zone (Atlantic Ocean), *Earth Planet. Sci. Lett.*, *146*, 273–287.

Shen, Y., and D. W. Forsyth (1995), Geochemical constraints on initial and final melting beneath mid-ocean ridges, *J. Geophys. Res.*, *100*, 2211–2237.

Sisson, T. W., and T. L. Grove (1993), Experimental investigations of the role of H_2O in calc-alkaline differentiation and subduction zone magmatism, *Contrib. Mineral. Petrol.*, *113*, 143–166.

Sobolev, A. V., and N. Shimizu (1993), Ultra-depleted primary melt included in an olivine from the Mid-Atlantic, *Nature*, *363*, 151–154.

Spiegelman, M., and P. B. Kelemen (2003), Extreme chemical variability as a consequence of channelized melt transport, *Geochem. Geophys. Geosyst.*, *4*(7), 1055, doi:10.1029/2002GC000336.

Thompson, R. N., I. L. Gibson, G. F. Marriner, D. P. Mattey, and M. A. Morrison (1980), Trace-element evidence of multistage mantle fusion and polybaric fractional crystallization in the Paleocene lavas of Skye, NW Scotland, *J. Petrol.*, *21*, 265–293.

Tormey, D. R., T. L. Grove, and W. B. Bryan (1987), Experimental petrology of normal MORB near the Kane Fracture Zone: 22°–25°N, Mid-Atlantic Ridge, *Contrib. Mineral. Petrol.*, *96*, 121–139.

Ulmer, P. (2001), Partial melting in the mantle wedge—The role of H_2O in the genesis of mantle-derived ‘arc-related’ magmas, *Phys. Earth Planet. Inter.*, *127*, 215–232.

Villiger, S., P. Ulmer, O. Müntener, and A. B. Thompson (2004), The liquid line of descent of anhydrous, mantle-derived, tholeiitic liquids by fractional and equilibrium crystallization—An experimental study at 1.0 GPa, *J. Petrol.*, *45*, 2369–2388.

Villiger, S., P. Ulmer, and O. Müntener (2007), Equilibrium and fractional crystallization experiments at 0.7 GPa—The effect of pressure on phase relations and liquid compositions of tholeiitic magmas, *J. Petrol.*, doi:10.1093/petrology/egl05 in press.

Weaver, J. S., and C. H. Langmuir (1990), Calculation of phase equilibrium in mineral-melt systems, *Comput. Geosci.*, *16*, 1–16.

Wendt, J. I., M. Regelous, Y. Niu, R. Hékinian, and K. D. Collerson (1999), Geochemistry of lavas from the Garret Transform fault: Insights into mantle heterogeneity beneath the eastern Pacific, *Earth Planet. Sci. Lett.*, *173*, 271–284.

White, R. S., R. S. Detrick, M. C. Sinha, and M. H. Cormier (1984), Anomalous seismic crustal structure of oceanic fracture zones, *Geophys. J. R. Astron. Soc.*, *79*, 779–798.

White, R. S., T. A. Minshull, M. J. Bickle, and C. J. Robinson (2001), Melt generation at very slow-spreading oceanic ridges: Constraints from geophysical data, *J. Petrol.*, *42*, 1171–1196.

Yang, H. J., R. J. Kinzler, and T. L. Grove (1996), Experiments and models of anhydrous, basaltic olivine-plagioclase-augite saturated melts from 0.001 to 10 kbar, *Contrib. Mineral. Petrol.*, *124*, 1–18.

O. Müntener, Institute of Mineralogy and Geochemistry, University of Lausanne, Anthropole, CH-1015 Lausanne, Switzerland. (othmar.muntener@unil.ch)

P. Ulmer and S. Villiger, Department of Earth Sciences, ETH Zurich, Clausiusstr. 25, CH-8092 Zurich, Switzerland.